Biogeosciences Discuss., https://doi.org/10.5194/bg-2018-411
Manuscript under review for journal Biogeosciences
Discussion started: 11 October 2018
© Author(s) 2018. CC BY 4.0 License.

Biogeosciences Discussions Open Access EGU

Patterns and drivers of dimethylsulfide concentration in the northeast Subarctic Pacific across multiple spatial and temporal scales

Alysia E. Herr[1], Ronald P. Kiene[2], John W. H. Dacey[3], Philippe D. Tortell[1,4,5]

[1]Department of Earth, Ocean and Atmospheric Sciences, University of British Columbia, Vancouver, BC, V6T 1Z4, Canada
[2]Department of Marine Sciences, University of South Alabama, Mobile, AL, 36688, USA
[3]Woods Hole Oceanographic Institute, Woods Hole, MA, 02543, USA
[4]Botany Department, University of British Columbia, Vancouver, BC, V6T 1Z4, Canada
[5]Peter Wall Institute for Advanced Studies, University of British Columbia, Vancouver, BC, V6T 1Z4, Canada

Correspondence to: Alysia E. Herr (aherr@eoas.ubc.ca)

Abstract. The northeast subarctic Pacific (NESAP) is a globally important source of the climate-active gas dimethylsulfide (DMS), yet the processes driving DMS variability across this region are poorly understood. Here we examine the spatial distribution of DMS at various spatial scales across contrasting oceanographic regimes of the NESAP. We present a new data set of high spatial resolution DMS measurements across hydrographic frontal zones along the British Columbia continental shelf, together with key environmental variables and biological rate measurements. We combine these new data with existing observations to produce a revised summertime DMS climatology for the NESAP, yielding a broader context for our sub-mesoscale process studies. Our results demonstrate sharp DMS concentration gradients across hydrographic frontal zones, and suggest the presence of two distinct DMS cycling regimes corresponding to microphytoplankton-dominated waters along the continental shelf, and nanoplankton-dominated cross-shelf transitional waters. DMS concentrations across the continental shelf transition (range <1–10 nM, mean 3.9 nM) exhibited positive correlations to salinity (r=0.80), sea surface height anomaly (SSHA; r=0.51) and relative prymnesiophyte abundance (r=0.88). In contrast, DMS concentrations in near shore coastal transects (range <1–24 nM, mean 6.1 nM) showed a negative correlation with salinity (r=-0.69, r=-0.78) and SSHA (r=-0.81, r=-0.75), and a positive correlation to relative diatom abundance (r=0.88, r=0.86). These results highlight the importance of bloom-driven DMS production in continental shelf waters of this region, and the role of prymnesiophytes in DMS cycling further offshore. In all areas, the rate of DMS consumption appeared to be an important control on observed concentration gradients, with higher DMS consumption rate constants associated with lower DMS concentrations. A compiled dataset of all available summertime DMS observations for the NESAP (including previously unpublished results) was used to examine the performance of several existing algorithms to predict regional DMS concentrations. We found that none of these existing algorithms was able to accurately reproduce observed DMS distributions across the NESAP, although performance was improved by the use of regionally tuned-coefficients. Based on our compiled observations, we derived an average summertime distribution map for DMS concentrations and sea–air fluxes across the NESAP. We estimated that this region emits 0.30 Tg of sulfur to the atmosphere during the summer season.

Biogeosciences Discuss., https://doi.org/10.5194/bg-2018-411
Manuscript under review for journal Biogeosciences
Discussion started: 11 October 2018
© Author(s) 2018. CC BY 4.0 License.

1 Introduction

Spurred by a proposed role in climate regulation as a source of cloud-condensation nuclei and back-scattering aerosols, the biogenic trace gas dimethylsulfide (DMS) and related organic sulfur compounds dimethylsulfoniopropionate (DMSP) and dimethyl sulfoxide (DMSO) have been studied for more than four decades (Lovelock et al. 1972; Charlson et al. 1987). This body of research has revealed complex sulfur biogeochemical cycling in the oceans, and important physiological and ecological roles for these molecules (Simó 2004; Stefels et al. 2007). DMSP and DMS have been shown to play an essential function in marine microbial systems as sources of carbon and sulfur (Kiene et al. 2000; Reisch et al. 2011). These molecules also act as olfactory foraging cues for numerous species of birds, fish, marine invertebrates and mammals (Seymour et al. 2010; Johnson et al. 2016), thereby driving interactions both within and beyond the marine microbial food web. The ecological, chemical and climatological significance of DMS and related compounds has stimulated significant effort to understand the surface ocean distribution of these molecules and the underlying factors driving their variability.

The Pacific Marine Environmental Laboratory (PMEL) has compiled a database of over 47,000 discrete DMS measurements. Lana et al. (2011) utilized these data to construct a global climatology of surface ocean DMS concentrations and sea–air fluxes, providing broad-scale understanding of oceanic distribution patterns. The global mean DMS concentration is estimated to be approximately 2 nM, but the climatology reveals several regional 'hot-spots' of elevated DMS accumulation, including the Southern Ocean and northeast Subarctic Pacific (NESAP), where surface ocean DMS concentrations 5–10-fold higher than the mean oceanic value are commonly observed. Although large-scale global patterns derived from the climatology are likely robust, a fuller understanding of spatial and temporal patterns of regional DMS variability is constrained by the relatively poor spatial and temporal coverage of existing measurements.

The NESAP, defined here as the region bounded by 44.5˚ N and 61˚ N latitude and 180˚ W and 120˚ W, exhibits consistently high summertime DMS concentrations in both open ocean and coastal regions, with maxima of ~20 nM observed during the late summer season (Wong et al. 2005; Asher et al. 2011, 2017; Steiner et al. 2012). This oceanic region is also characterized by strong spatial heterogeneity of environmental characteristics. High-productivity coastal upwelling regions transition to iron-limited high nutrient low chlorophyll (HNLC) waters offshore (Boyd and Harrison 1999; Boyd et al. 2004). Seasonally varying surface currents, fresh water inputs, coastal upwelling and recurrent formation of westward-propagating mesoscale eddies result in semi-permanent and transient hydrographic frontal zones, impacting regional marine biodiversity and productivity (Crawford et al. 2005; Whitney et al. 2005; Ribalet et al. 2010). This spatial heterogeneity makes it challenging to quantify DMS distributions from discrete ship-based sampling, and complicates region-wide generalizations of DMS dynamics.

Recent work has highlighted differences in the distribution of DMS and related compounds across distinct domains of the NESAP, particularly in offshore and coastal regions (Wong et al. 2005; Asher et al. 2011, 2017; Steiner et al. 2012). The

© Author(s) 2018. CC BY 4.0 License.

HNLC offshore region was identified by L11 as an area of high DMS concentrations and sea–air fluxes. Results from in situ observations (Wong et al. 2005; Levasseur et al. 2006; Merzouk et al. 2006; Asher et al. 2011) and numerical models (Steiner et al. 2012) suggest that elevated DMS concentrations in these open ocean waters are driven by the presence of high DMS/P producing phytoplankton taxa, such as prymnesiophytes and dinoflagellates, and the effects of mixed layer stratification and Fe-limitation, which may act to increase DMS/P production as a means to offset oxidative stress (Sunda et al. 2002). A low particulate carbon to organic sulfur ratio in the HNLC regime further influences bacterial DMSP metabolism, resulting in increased DMS-yield from DMSP metabolism (Merzouk et al. 2006; Royer et al. 2010). In the physically dynamic coastal waters of the NESAP, high DMS concentrations likely result, in part, from seasonal coastal upwelling, which drives high phytoplankton biomass accumulation. Indeed, recent work (Asher et al. 2017) has demonstrated an enhancement of DMS accumulation following upwelling events, consistent with previously observed high DMS/P concentrations in upwelling regions (Hatton et al. 1998; Zindler et al. 2012; Wu et al. 2017). Increased DMS concentrations in the post-upwelling bloom phase may result from nitrogen limitation, increased grazing pressure (which releases DMSP into the dissolved pool), oxidative stress associated with shoaling mixed layers, and a phytoplankton community shift towards high DMSP-producing species (Nemcek et al. 2008; Franklin et al. 2009).

New advances in sensor technology over the past decade have begun to significantly expand DMS data coverage in a number of ocean regions. These fine scale measurements reveal novel features and highlight the apparent influence of oceanographic frontal zones in driving fine-scale DMS distribution patterns (Locarnini et al. 1998; Tortell 2005a; Nemcek et al. 2008; Jarníková et al. 2018). In previous work (Asher et al. 2017), we have documented sharp transitions in DMS concentrations across salinity frontal zones in nearshore NESAP waters. This earlier work did not include corresponding measurements of DMS/P turnover rates, limiting mechanistic interpretation of the observed spatial patterns. To our knowledge, there has been no systematic evaluation of the processes driving fine-scale DMS variability across frontal zones. Such a study requires high resolution concentration measurements together with assessments of biological productivity and DMS/P turnover rates.

In this article, we present a new data set of DMS/P concentrations across coastal and open ocean waters of the Subarctic Pacific, from the northern Gulf of Alaska to the Oregon coast. Using a suite of measurements collected during two summer cruises (2016–2017), we document regional-scale features, and characterize sub-mesoscale DMS structure across hydrographic frontal zones in on-shelf and transition regions. Using real-time ship-board measurements, we were able to select contrasting sites across frontal zones for more extensive sampling and analysis, allowing us to probe underlying rate processes in adjacent areas of contrasting DMS/P concentrations and surface water hydrography. We combined our new data set with existing observations from our own group and from the existing PMEL database to produce a new summertime DMS climatology for the NESAP. This updated climatology enables us to better constrain the summertime distribution of DMS in the NESAP, identifying persistent DMS 'hot spots', and exploring correlations between DMS concentration and other biotic

© Author(s) 2018. CC BY 4.0 License.

and abiotic variables. We use our compiled data set to evaluate various empirical algorithms predicting DMS concentrations and sea–air fluxes across the NESAP. Our results yield new insights into the spatial patterns and potential drivers of summertime NESAP DMS distribution across various spatial scales in a globally important oceanic region.

2 Methods

2.1 Data overview

In this study, we combined new data from two recent oceanographic expeditions with existing observations derived from several decades of compiled DMS measurements in the NESAP. Ancillary data (e.g. environmental and biological variables) were obtained from a number of sources (both ship-based measurements, remote sensing and blended data products) to help interpret DMS distribution patterns. The various data sets are described below.

2.2 New high-resolution data sets

2.2.1 Underway ship-board measurements

Field sampling was conducted on board the University–National Oceanographic Laboratory System (UNOLS) vessel R/V *Oceanus* during July of 2016 and August of 2017 (O16, O17, respectively). Our cruise tracks included offshore, coastal and transitional waters throughout the Gulf of Alaska (Fig. 1). We define the coastal regime as those waters with bottom depths shallower than 2000 m, as per Asher et al. (2011). We utilized real-time DMS measurements (see below) and NASA satellite ocean color imagery (AquaMODIS) to guide our cruise track, enabling us to identify areas with high concentrations of DMS and strong spatial gradients in surface water phytoplankton biomass and hydrography (sea surface temperature and salinity). During O16 we also conducted detailed surveys of three hydrographic frontal zones that exhibited sharp DMS concentration gradients. One of these surveys (T1; Fig. 1) was located in the coastal-open ocean transition near Dixon Entrance north of Haida Gwaii (formerly the Queen Charlotte Islands), while the other two transects were located along the British Columbia continental shelf (T2: Hecate Strait and T3: La Perouse Bank; Fig. 1). After an initial survey to examine frontal structure, stations were selected for depth-resolved sampling to cover the gradients present across the frontal zone. The O17 cruise covered a similar area as O16. Although we did not perform detailed transect surveys on this second cruise, we did sample waters near T1–T3.

High resolution surface water DMS measurements were conducted using membrane inlet mass spectrometry (MIMS) following published methods (Tortell 2005b; Nemcek et al. 2008). The MIMS system, utilizing the ship's underway seawater flow through system (~5 m intake depth), allows for high-frequency sampling (2–3 times per minute), yielding a spatial resolution of ~150–200 m at normal ship speeds (8–10 kts). During these cruises, DMS concentrations were also measured in discrete water samples collected at 5 m depth using a purge-and-trap system connected to a gas chromatograph equipped with

© Author(s) 2018. CC BY 4.0 License.

a flame-photometric detector (FPD-GC) (Kiene and Service 1991). These discrete measurements were used to assess the accuracy of MIMS-based measurements. We found good agreement between methods, with a mean absolute error of 0.93 nM between the two instruments across the full range of measured concentrations (Fig. 2).

High resolution DMS measurements were paired with ancillary underway data and rate measurements to examine potential drivers of spatial variation. A ship board thermosalinograph was used to measure sea surface temperature (SST) and salinity at high spatial resolution (SBE 45 and SBE 38 for salinity and temperature, respectively). Chlorophyll-*a* (chl-*a*) concentration was measured using a WET labs ACS absorbance/attenuation meter, based on the absorption line height at 676 nm (Bricaud et al. 1995; Roesler and Barnard 2013; Burt et al. 2018). These chl-*a* concentrations were further used to derive an estimate of phytoplankton size and taxonomic distributions, based on the empirical algorithm of Hirata et al. (2011). Zeng et al. (2018) have recently demonstrated the efficacy of this algorithm in our region as validated against HPLC-pigment-derived phytoplankton taxonomy data (detailed below), and we used the empirical coefficients for this model tuned specifically for the NESAP. MIMS was also used to determine the ratio of oxygen and argon concentrations relative to atmospheric saturation. The resulting biological oxygen saturation term, $\Delta O_2/Ar$, can be used to calculate net community productivity (NCP) from the air–sea gas exchange of O_2 (Kaiser et al. 2005). We used the calculation approach of Reuer et al. (2007) to compute NCP from our $\Delta O_2/Ar$ measurements. We note that some of these estimates, particularly in regions of active upwelling, are likely biased by the entrainment of O_2 under-saturated water into the mixed layer. While this effect can be accounted for using N_2O measurements (Izett et al. 2018), we do not have these data available for our cruises. Our derived NCP estimates thus likely represent under-estimates, and we have removed all negative NCP values. Nonetheless, the general spatial patterns we observed in NCP are likely to be robust.

2.2.2 Station-based measurements

We measured a suite of variables at selected sampling stations along the cruise track. All water for ancillary measurements was taken from 5 m depth, collected using Niskin bottles. A Seabird CTD probe (Seabird 911plus) was deployed at each station to obtain depth profiles of hydrographic features over the upper 200 m of the water column. A density difference criterion of 0.05 kg m^{-3} was used to calculate mixed layer depths.

DMS loss and DMSP consumption rates were measured using the radio-labeled ^{35}S methods outlined by Kiene and Linn (2000). Briefly, ^{35}S-labeled DMSPd or DMS were added to samples at non-perturbing concentrations (<1 % of ambient levels). Samples were incubated in the dark at surface water temperatures for <1 h (^{35}S-DMSP) or <7 h (^{35}S-DMS). The rate constant for DMSPd turnover was determined by measuring the disappearance of ^{35}S-DMSP from the dissolved (< 0.2 µm) pool. The rate constants for DMS loss were determined by measuring the accumulation of dissolved, non-volatile ^{35}S transformation products of the volatile ^{35}S-DMS tracer. Consumption rates (nmol L^{-1} d^{-1}) were calculated by multiplying in situ DMS or DMSPd concentrations by the measured rate constant (k_{DMS} or k_{DMSPd} respectively).

© Author(s) 2018. CC BY 4.0 License.

Primary productivity was measured using 24 h ^{14}C uptake incubations, following the method outlined by Schuback et al. (2015). Incubation bottles were held in a deck-board incubator plumbed with continuously flowing seawater to achieve in situ temperature. The light intensity was adjusted to ~ 30 % surface irradiance enriched in blue light using neutral density screening in combination with blue photographic film (LEE filters: #209 and CT blue maximum transmission at approx. 460 nm). Light levels in the tank were measured with a ULM-500 light meter equipped with a 4π-sensor (Walz). Bacterial production was measured using the tritiated leucine method (Smith and Azam 1992). Station samples were also analyzed for total and dissolved DMSP (DMSPt and DMSPd) using the previously described NaOH cleavage and small-volume gravity drip filtration method (Dacey and Blough 1987; Kiene and Slezak 2006).

We obtained discrete estimates of phytoplankton assemblage composition using diagnostic pigment analysis (DPA) based on measurements of photosynthetic pigments using HPLC analysis. For these measurements, 1 L sampled were collected on GF/F filters (nominal pore size ~ 0.7 µm), flash frozen in liquid nitrogen and stored frozen until analysis in the laboratory. The DPA method was originally developed by Vidussi et al. (2001), and subsequently refined (Uitz et al. 2006; Hirata et al. 2008; Brewin et al. 2010) to more accurately capture phytoplankton type and size class. The estimation formulas here are those of Hirata et al. (2011). Percent contribution to phytoplankton assemblage was assessed for three size classes (micro-, nano-, and pico-) and several taxonomic groups, including diatoms, dinoflagellates and prymnesiophytes.

2.3 Compilation of published data

To provide a broader regional spatial context for our observations, we combined discrete DMS measurements from the PMEL data archive with high spatial resolution DMS measurements made using MIMS since the early 2000s. Table 1 provides dates and spatial domains of the cruises, along with relevant literature citations. Note that some of the DMS data included in this compilation have not been previously published. All of our compiled MIMS data have been made available on the PMEL database.

2.3.1 MIMS data sets

MIMS-based observations included in this study are derived from 11 cruises conducted between 2004 and 2017, primarily aboard the Canadian Coast Guard Ship *John P. Tully* as part of ongoing time-series monitoring programs conducted by the Department of Fisheries and Oceans Canada (DFO). Only summertime data (defined here as June, July and August) falling within the NESAP region (44.5°–61° N, 180°–120° W) were included in this compilation. All measurements were binned to a temporal sampling resolution of 1 minute. The cruises VIJ04, VIJ10, WCAC10, LPA11, O16 and O17 include paired NCP values obtained from MIMS measurements, using the $\Delta O_2/Ar$-based method described above. All DMS data points are paired with shipboard sea surface salinity and SST.

© Author(s) 2018. CC BY 4.0 License.

2.3.2 PMEL data extraction

We accessed the PMEL data base (http://saga.pmel.noaa.gov/dms/) on 6 December, 2017 to extract observations from June, July and August in the NESAP region defined above. Our selection criteria yielded 3236 data points between 1984 and 2003. These observations were relatively evenly distributed between the three months, but were biased spatially, with a preponderance of data derived from on-shelf waters off the coast of Alaska (see Fig. 8b). As with MIMS data, each data point includes paired sea surface salinity and SST measurements.

2.4 Ancillary measurements

Ancillary oceanographic data were used to contextualize DMS spatial distributions, examine potential correlations to environmental variables and evaluate the performance of several empirical algorithms predicting DMS concentrations. In many cases, ancillary variables of interest (e.g. chl-*a*) were not reported in conjunction with DMS data, and we thus utilized a number of remote sensing data products, as described below. Remotely-sensed parameters were linearly interpolated to the spatial resolution of ship-based DMS observations.

AquaMODIS satellite data were used to obtain information on photosynthetically available radiation (PAR), chl-*a* (OCI algorithm), calcite (Gordon et al. 2001; Balch et al. 2005) and diffuse attenuation coefficients (Werdell and Bailey 2005). For these data products, we extracted level 3 gridded data from http://oceancolor.gsfc.nasa.gov/cgi/l3 at 9 km resolution. Monthly means for chl-a, calcite and k_d were utilized to maximize spatial coverage, whereas 8 day average PAR data were used. AquaMODIS chlorophyll data were also used to calculate sea surface nitrate (SSN) using a North Pacific-specific algorithm based on chl-*a* and SST (Goes et al. 2000). Aqua MODIS data are only available starting in July of 2002, whereas most of the PMEL data set in this region is from sampling prior to 2003. For earlier observations, we used chl-*a* data from the SeaWiFS satellite.

We obtained information on sea-surface height anomalies (SSHA) using gridded data sets (5 day, 0.17° x 0.17° resolution) obtained from ftp://podaac-ftp.jpl.nasa.gov/allData/merged_alt/L4/cdr_grid_interim. This level 4 satellite product is derived from various sensors, and data are not available before 1992. Mixed layer depths at a monthly, 1˚ resolution were obtained from the China Second Institute of Oceanography (CSIO) ftp://data.argo.org.cn/pub/ARGO/BOA_Argo/. These data are based on gridded Argo float data produced using the Barnes method, and are available for the years 2004–present (Li et al. 2017). Due to limitations in Argo operational depths, data are largely absent from waters shallower than 2000 m.

We calculated sea–air DMS fluxes from DMS concentration data and surface wind-speeds using the gas transfer parameterization of Sweeney et al. (2007) and the Schmidt number formulation of Saltzman et al. (1993). Wind speed data for flux calculations were obtained from the NCEP/NCAR reanalysis dataset

© Author(s) 2018. CC BY 4.0 License.

(https://www.esrl.noaa.gov/psd/data/gridded/data.ncep.reanalysis.pressure.html) at a 2.5° daily resolution. Following previous studies, we assume negligible atmospheric DMS concentrations for our calculations, leading to a potential (though likely small) overestimate of the sea–air flux. For purposes of comparison to fluxes, we calculated DMS column burden along transects by multiplying DMS concentration and average mixed layer depth.

2.5 Data binning and province assignment

High resolution, underway measurements may introduce sampling biases due the large number of data points collected. For example, a ship holding station will increase spatial data density at a particular location, and the large number of observations can exert a disproportionate influence on derived mean values. To address this, all measurements in the data set were assigned to 1° spatial bins, in which all observations for a given year were averaged. The resulting yearly data grids were then averaged to create long-term gridded means. This technique effectively assigns equal weight to each year of measurements in a given grid cell. Both DMS and paired ancillary parameters were binned using this method.

Following the approach of L11, data grid cells were assigned to Longhurst's Biogeochemical Provinces to examine patterns across different regimes within the greater NESAP (Longhurst 2007). Three primary provinces fall within the domain of our study region: California Upwelling Coastal Province (CCAL), Alaska Downwelling Coastal Province (ALSK), and Pacific Subarctic Gyres Province – East (PSAE) (Fig. 8). The CCAL province as defined by Longhurst extends south to 16.5° N. Hereafter, all references to the CCAL refer to the portion of this province above 44.5° N latitude. Province boundary designations were obtained from www.marineregions.com (accessed October 2017), and the MATLAB native inpolygon.m function was used to assign grid cells to individual provinces. Any grid cell either inside or on the edge of boundaries was assigned to a particular province. As such, some data cells (37 out of 216 total) are assigned to multiple provinces. Average summer DMS concentrations and flux measurements were computed for each province. For comparison to L11, we recalculated the average summertime DMS concentration and flux in the three study provinces using only the PMEL data utilized by Lana et al. (2011). Data were first binned using the year-weighted method described above.

2.6 Statistical analysis and empirical algorithms

We used our compiled data set to examine broad-scale relationships between DMS and other oceanographic variables. For this analysis, data were log-transformed to overcome non-normal distributions, and the strength of pair-wise relationships was assessed by computing Pearson's correlation coefficients. Correlations were applied to 1˚ x 1˚ binned data both within individual provinces and across the entire NESAP.

We also used several existing empirical algorithms to reconstruct DMS fields at a 1˚ x 1˚ resolution from various environmental predictor variables, comparing the accuracy of the resultant products against our binned DMS observations. The algorithms tested in this study include that of Simó and Dachs (2002), Vallina and Simó (2007), and Watanabe et al. (2007) (hereafter,

© Author(s) 2018. CC BY 4.0 License.

SD02, VS07, and W07, respectively). Both SD02 and VS07 used global data bases to develop their algorithms. SD02 relates DMS to chl-*a*:MLD, with chl-*a* values > 15 µg L^{-1} removed prior to analysis. VS07 relates DMS concentration to solar radiative dose (SRD). This term, as defined by the authors, is based on light extinction coefficients (k_d), sea surface irradiance (I_0), and mixed layer depth. Due to the large areal extent of the study area, we used AquaMODIS derived PAR in lieu of the station-based I_0 measurements used by the authors. Similarly, strong variation in k_d in coastal vs. open ocean waters is expected. We thus modified the author's approach and used satellite derived k_d (based on a chlorophyll-dependent algorithm; Werdell and Bailey 2005) rather than a fixed coefficient. W07 uses data specific to the North Pacific and relates DMS to SST, SSN and latitude. Recognizing the utility of re-parameterizing proposed algorithms for specific areas, we tested all algorithms using both published linear coefficients, and coefficients derived specifically for the NESAP observations using a least-squares approach to determine best fit to our data set.

3 Results

We begin by presenting an overview of our new DMS measurements and ancillary data from the 2016–2017 summer cruises, highlighting DMS distributions and the presence of distinct surface water properties across different parts of our transect. We then provide a detailed description of DMS dynamics across several hydrographic frontal zones, discussing the potential role of various processes in driving these gradients. Finally, we construct an updated summertime climatology for this region, compiling our new measurements with existing DMS observations from across the NESAP to examine large-scale patterns in DMS distributions, and correlations with other oceanographic variables. The potential role of these variables in driving DMS distributions in the NESAP, and the need for additional process studies is addressed in the discussion.

3.1 Oceanographic conditions in the NESAP during summer 2016–2017

Our 2016 and 2017 cruises surveyed oceanographic regimes from offshore HNLC regions to productive coastal upwelling zones. As indicated by AquaMODIS satellite imagery, chl-*a* concentrations exhibited strong gradients across the oceanic-coastal transition in both 2016 and 2017 (Fig. 1). Coastal waters showed elevated chl-*a*, with maximum values of 50 µg L^{-1} and 18 µg L^{-1} in 2016 and 2017, respectively. In both years, highest chl-*a* values were observed in waters with shallow mixed-layer depths (<10 m) along the La Perouse Bank (Fig. 1). In the off-shelf regions, chl-*a* concentrations appeared uniformly low in 2016, although significant cloud cover limited the availability of satellite imagery. By comparison, we observed generally higher chl-*a* concentrations in offshore waters in 2017. Most notably, our cruise track passed through a likely coccolithophore bloom in the northern Gulf of Alaska, where a large apparent calcite signal (~2 mmol PIC m^{-3}) was detected in AquaMODIS imagery. Patterns in NCP were generally similar to those of chl-*a*, with elevated production in coastal waters (Fig. 2c). In both years, we observed NCP on La Perouse Bank exceeding 100 mmol O_2 m^{-2} d^{-1} (Fig. 2c, inset).

© Author(s) 2018. CC BY 4.0 License.

Coastal regions exhibited generally fresher surface waters and shallower mixed layer depths, except for several regions of enhanced vertical mixing associated with upwelling. This coastal upwelling signature was apparent in elevated salinity and decreased temperature of surface waters, and also through the presence of negative sea surface height anomalies (Fig. 1c,d). Small-scale regional heterogeneity in coastal regions was apparent in both years, with salinity and temperature exhibiting sharp gradients over the continental shelf, associated with riverine input and complex mixing processes. By comparison, oceanic surface waters showed less spatial heterogeneity, and were generally more saline, with deeper mixed layers (Fig. 2b). The sea-surface height anomaly field indicated the presence of several Sitka and Haida eddies in both years (Fig. 1c,d), enhancing mesoscale variability through the transport of coastal water offshore.

Using the approach of Hirata et al. (2011) and Zeng et al. (2018), we derived high resolution estimates of phytoplankton assemblage composition from our underway chl-*a* measurements. This approach revealed a predominance of phytoplankton in the micro- size class (>20 µm) in coastal waters (Fig. 2d), with an average of 50 % of chl-*a* attributable to microphytoplankton. In contrast, off-shelf waters showed greater diversity in phytoplankton composition. In these waters, microphytoplankton accounted for ~25 % of total chl-*a*, while the pico- and nano- size classes accounted for ~30 % and ~40 %, respectively (Fig. 2e,f).

3.2 DMS distributions

Across our study region, surface water DMS concentrations ranged from <1–24 nM in 2016 and <1–18 nM in 2017 (Fig. 2a, Fig. 3). The average DMS concentrations showed very small (though statistically significant) difference between years (2.8 nM median, 1.0 – 5.7 interquartile range in 2016 and 2.6 nM median, 1.8 – 4.0 interquartile range in 2017; $p<0.001$ using Wilcoxon rank sum test). We observed a number of localized DMS 'hot spots' in regions of elevated chl-*a* and NCP. In both years, these localized high DMS regions were particularly evident in the vicinity of the highly productive La Perouse Bank (Fig. 2a, inset). We also observed several areas where strong DMS gradients co-occurred with salinity fronts. These areas include the T1–T3 transects survey in O16, detailed below. Despite associations between DMS concentration and several variables in some localized regions, we only observed weak correlations between DMS and other measured variables across the full cruise tracks. During O16, DMS concentrations were most strongly correlated to NCP, with a Pearson's coefficient of $r=0.42$ ($p<0.001$). This relationship was substantially weaker in O17 ($r=0.29$, $p<0.001$).

3.3 Detailed surveys of DMS across hydrographic frontal zones

During the O16 cruise, we sampled along three repeated transects to map DMS distributions near hydrographic frontal zones. All three transects showed significant gradients in salinity, chl-*a* and DMS/P concentrations, as well as in the metabolic activity of phytoplankton and bacteria (Fig. 4, 6–7). While DMS concentrations appeared to co-vary with salinity and chl-*a* across

© Author(s) 2018. CC BY 4.0 License.

these frontal zones, the strength and direction of these relationships were not consistent across the three transects. We discuss each transect in detail below.

3.3.1 Transect 1

T1 was located west of Dixon Entrance (Fig. 1) in waters influenced by the Alaska Current and coastal water masses. Offshore waters along this transect were more saline and colder than those on the shelf. The area exhibited DMS concentrations up to 10 nM in off-shelf, saline waters (Fig. 4). At the shelf break (approx. 134.4° W, indicated on Fig. 4 by dotted line), we measured a sharp drop in salinity and corresponding decrease in DMS concentrations, with concentrations remaining below ~3 nM over the most coastal parts of the transect. Across the entire T1 transect, DMS concentrations displayed a striking fine-scale coherence to salinity ($r=0.80$, $p<0.001$; Fig. 4a,b). A significant positive correlation was also observed with SSHA ($r=0.51$, $p<0.001$), indicating a potential influence of westward-propagating Haida eddies. Fig. 5 shows a line plot of SSHA measurements from the approximate time of T1 sampling, overlaid by DMS concentrations. Despite differences in spatial resolution, the coherence between DMS concentrations and mesoscale oceanographic features can be seen in this figure.

The lower salinity coastal waters were characterized by elevated chl-*a* concentrations (Fig. 4c), resulting in a negative correlation between DMS concentrations and chlorophyll ($r=-0.47$, $p<0.001$). Figure 4c shows the estimated percent abundance of prymnesiophytes and diatoms as derived from HPLC-based DPA-analysis. Although HPLC samples are not available for all of the coastal waters we sampled, results obtained from the empirical algorithm of Hirata et al. (2011) suggest a shift in phytoplankton assemblage composition between smaller size classes in offshore waters to a microphytoplankton-dominated community in on-shelf waters. DMS exhibited relatively weak, though statistically significant ($p<0.001$) positive correlations with the derived abundance of nano- and picophytoplankton size-classes ($r=0.55$ and $r=0.38$, respectively), and a negative correlation with the relative abundance of microphytoplankton ($r=-0.53$). In support of this result, HPLC measurements revealed a strong positive relationship between DMS concentration and relative abundance of prymnesiophytes ($r=0.88$, $p=0.002$), and a negative correlation to diatom abundance ($r=-0.70$, $p=0.036$). Moreover, we observed a strong positive correlation between DMS and DMSPt:chl-*a* ($r=0.80$, $p=0.003$) suggesting higher cellular DMSP concentrations in phytoplankton assemblages in the off-shelf regions of this transect. Overall, results from this transect demonstrate a transition from high DMS concentrations in the lower productivity, nano-plankton dominated offshore waters, to low DMS concentrations in higher productivity, diatom-dominated nearshore region.

Rate constants (d^{-1}) for biological consumption of both DMS and DMSPd were higher in the on-shelf region (although the on-shelf/off-shelf difference was only statistically significant for k_{DMSPd}), signifying faster removal of DMS/P from coastal surface waters with lower DMS concentrations. For DMS and DMSPd respectively, loss constants averaged 1.15 ± 0.3 d^{-1} and 88.2 ± 13.9 d^{-1} onshore, as compared to 0.66 ± 0.045 d^{-1} and 39.6 ± 1.45 d^{-1} in offshore stations (Fig. 4e). Net primary productivity and bacterial productivity were also higher, on average, in the low DMS coastal waters, but these differences were not

© Author(s) 2018. CC BY 4.0 License.

statistically significant. These results suggest that enhanced microbial activity and relatively higher DMS/P consumption rate constants played a role in maintaining lower concentrations of these compounds in nearshore waters.

We calculated the mixed layer DMS burden by multiplying concentration and average mixed layer depth (13 m). Biological DMS loss integrated over the mixed layer averaged 22 μmol m^{-2} d^{-1}, sufficient for daily removal of 47 % of the DMS burden. By comparison, derived sea–air flux estimates across the transect exhibited a mean value of 13 μmol DMS m^{-2} d^{-1}. Using this value, we found that DMS loss to sea–air flux could on average remove 26 % of mixed layer DMS burden daily, given no new production. Due to a relatively homogenous wind field over the area of our sampling transect, the sea–air fluxes were tightly correlated to DMS concentrations, such that the lower DMS concentrations in nearshore regions cannot be explained by greater rates of ventilation to the atmosphere.

3.3.2 Transect 2

The second sampling transect, T2, was located in the coastal waters of Hecate Strait situated on the continental shelf (Fig. 1). Sea surface temperatures along this transect showed small variation (standard deviation ~0.5˚ C), with the lowest temperature waters located mid-transect in areas of highest chl-*a*. Mixed layer depths ranged from 10–15 m, and DMS concentrations ranged from < 0.5 nM to nearly 20 nM (Fig. 6). In contrast to our observations for T1, DMS concentrations exhibited negative correlations to both salinity ($r=-0.69$, $p<0.001$; Fig. 6b) and SSHA ($r=-0.81$, $p<0.001$) in this area. Despite the small absolute change in salinity across this transect (< 0.4 psu), we observed strong coherence of DMS to salinity structure. In contrast to T1, however, DMS concentrations were not significantly correlated to chl-*a* (Fig. 6c). Despite lack of correlation to chl-*a,* DMS did exhibit significant, though weak, positive correlations with estimates of relative microphytoplankton abundance ($r=0.22$, $p<0.001$), and stronger negative correlations with the abundance of pico- and nano- size classes (T2: $r=-0.47$, $r=-0.45$; $p<0.001$; Fig. 6c). In support of this observation, HPLC-pigment data revealed a strong positive relationship between DMS concentration and relative abundance of diatoms derived ($r=0.88$, $p=0.001$), and a negative correlation between DMS and prymnesiophyte abundance ($r=-0.77$, $p=0.010$). These correlations thus suggest diatoms as an important source of DMS, a result that is opposite to that observed for T1.

Unlike bulk chl-*a* concentrations, we found that primary productivity showed a strong positive correlation with DMS along T2 ($r=0.90$, $p=0.037$), although this result is based on only four data points. Bacterial productivity was also significantly higher in the high DMS waters, although this variable was even more sparsely sampled along the transect, and we cannot infer any meaningful statistical association with DMS (Fig. 6f). As with T1, both k_{DMSPd} and k_{DMS} were higher in the low-DMS portions of the transect. Across the entire transect, consumption values ranged from 0.51 to 1.29 d^{-1} for k_{DMS} and 28.8 to 49.5 d^{-1} for k_{DMSPd} (Fig. 6e). This result suggests microbial consumption as potential driver of DMS distributions, with higher DMS/P consumption rate constants in waters with lower DMS concentrations.

© Author(s) 2018. CC BY 4.0 License.

Integrated biological DMS loss was significantly higher than that of T1, with an average 78 µmol m^{-2} d^{-1} (equivalent to removal of 87 % of the DMS burden per day). By comparison, DMS sea-air flux across the transect was low, with a mean value of 2.9 µmol m^{-2} d^{-1}. This flux was sufficient to remove only ~6 % of mixed layer DMS burden daily. As with T1, the spatial pattern of sea-air flux was tightly correlated with DMS concentrations, and can thus not explain the observed DMS distribution patterns (i.e. higher sea-air flux in regions of high DMS concentrations). We thus conclude that DMS turn-over along this transect was dominated by biological processes.

3.3.3 Transect 3

T3 was located in the highly productive coastal waters of La Perouse Bank, along the continental shelf of the west coast of Vancouver Island (Fig. 1). Mixed layer depths ranged from 8–12 m, with the shallowest values found in fresher, salinity-stratified inshore waters influenced by riverine input. Sea surface temperature was lower in these fresher waters, although it varied little over the transect (standard deviation < 1˚ C). With respect to other measured variables, DMS behaved similarly to the coastal T2 transect (Fig. 7a). We observed a negative correlation between DMS and salinity ($r=-0.78$, $p<0.001$; Fig. 7b). We also found elevated chl-*a* in the low salinity waters, although there was only a weak positive correlation between chl-*a* and DMS ($r=0.25$, $p<0.001$) across the transect (Fig. 7c). A significant negative correlation was found between DMS and SSHA ($r=-0.75$, $p<0.001$).

Microphytoplankton dominated the low-salinity, high-DMS waters of the transect, with a shift towards smaller cells observed in the more saline waters farther offshore (Fig. 7c). Similar to T2, we found a significant positive correlation between DMS and microphytoplankton ($r=0.90$, $p<0.001$), and a negative correlation between DMS and phytoplankton of the nano- and pico-size class ($r=-0.77$, $r=-0.75$; $p<0.001$). In support of this observation, HPLC-pigment data showed a strong positive relationship between DMS concentration and relative abundance of diatoms ($r=0.86$, $p=0.003$), and a negative correlation with prymnesiophyte abundance ($r=-0.75$, $p=0.019$). A negative relationship was also observed between DMSPt:chl-*a* and DMS ($r=-0.88$, $p=0.002$) (Fig. 7d). In contrast to T1, high DMS coincided with regions of lower cellular DMSP concentrations among phytoplankton, consistent with the dominance of diatoms in the high DMS portions of this transect.

Along the T3 transect, DMS showed a positive association with primary productivity and bacterial productivity, though these relationships are based on very few sampling points. It is noteworthy that the bacterial productivity measured along T3 was higher than anywhere else along the cruise track, with production more than 5-fold greater than the cruise-wide average. Values of k_{DMS} ranged from 0.8–2.7 d^{-1} across the transect. As with T1 and T2, k_{DMS} was higher in low-DMS regions of T3. In contrast, k_{DMSPd} values along T3 increased in parallel with DMS concentrations (higher rate constants in higher DMS waters). DMSP loss constants ranged from 38.6 to 92.1 d^{-1} (Fig. 7e). The highest DMSP loss constant translates into a derived turnover time of just 16 minutes.

Biogeosciences Discuss., https://doi.org/10.5194/bg-2018-411
Manuscript under review for journal Biogeosciences
Discussion started: 11 October 2018
© Author(s) 2018. CC BY 4.0 License.

Biological DMS loss integrated over the mixed layer was sufficiently high to remove >100 % of the DMS burden daily (~47 μmol m^{-2} d^{-1}). Sea–air fluxes were a minor loss term by comparison (4.9 μmol m^{-2} d^{-1}), and were sufficient to remove only ~12 % of the mixed layer DMS burden. Due to low removal rates and relative homogeneity of wind speed fields, sea–air flux cannot be invoked to explain the spatial distribution of DMS across this transect.

3.4 Regional DMS distribution – comparisons of 2016 and 2017 observations with past studies

To explore potential regional-scale relationships between DMS concentrations and other environmental variables, we combined our new DMS data with measurements collected over the past three decades, including previously unpublished high-resolution MIMS data. The addition of new measurements to the existing PMEL data set substantially increases spatial and temporal coverage in the NESAP. When data were binned to 1˚ x 1˚ resolution, coverage was increased by ~20 % in the CCAL and ALSK Longhurst provinces, and 14 % in the PSAE, with the overall addition of 90 data-containing grid cells (Table 2). As shown in Fig. 8, our measurements primarily increase data coverage in waters below 57˚ N. These regions were previously under-sampled in the PMEL data set utilized by L11, which was strongly biased to measurements near the coast of Alaska. Figure 9a further illustrates the latitudinal shift in data coverage with the inclusion of additional MIMS data. As shown in Fig. 9b, average derived DMS concentrations across latitudinal bands at the north and south extremes of our study area remain similar to those derived from the PMEL data set utilized by L11. However, in the region between 50˚ N and 54˚ N, where there were few observations in the PMEL database, our compiled data show mean concentrations as much as 4.5 nM (~40 %) lower than those calculated using PMEL data alone.

Table 3 shows the change in province-wide average DMS concentration, sea–air fluxes, and total summertime DMS flux based on our updated analysis. Relative to our revised estimates, DMS concentration and flux derived using only the PMEL data were lower in the CCAL and higher in both the PSAE and ALSK provinces. The most pronounced difference was that of sea–air flux in the PSAE, where estimated sea–air fluxes decreased by 4.5 μmol m^{-2} d^{-1} (20 %). Despite these regional differences, the total summer DMS flux across the NESAP differed by only 6.5 % between our compiled data set (0.30 Tg S) and the PMEL data set utilized by L11 (0.32 Tg S).

Our compiled data set provides greater confidence in DMS concentrations and sea–air fluxes across the NESAP, and enables us to better constrain spatial patterns. Figure 10 shows binned average summertime DMS concentration across the region, as well as the derived sea–air DMS fluxes. The highest concentrations are observed in ALSK, where coastal waters contain maximum DMS concentrations exceeding 20 nM. A persistent region of elevated DMS concentrations is also evident in mid-PSAE oceanic region, with concentrations greater than 10 nM. Sea–air DMS fluxes show a similar spatial distribution as

© Author(s) 2018. CC BY 4.0 License.

DMS concentrations, with maximum values of >100 μmol m^{-2} d^{-1}. We also calculated and DMS:chl-*a* ratio for binned data (Fig. 10c), showing generally higher ratios in offshore NESAP waters.

3.5 Correlations and algorithm testing

Using our new data compilation, we examined the relationship between DMS concentrations and a suite of oceanographic variables across the NESAP. Table 4 shows both NESAP-wide and province-specific correlations derived from this analysis. While many correlations are weak or not statistically significant, some patterns do emerge, particularly in the offshore waters of the PSAE domain. No single variable explains a large portion of the DMS variation in this province, but statistically significant correlations exist between DMS and chl-*a* and calcite (r=0.45 and r=0.50, respectively). We also found a negative relationship between DMS and SSHA (r=-0.47). For the ALSK province, we found weak inverse correlations between DMS and SST (r=-0.32) and water depth (r=-0.34). Significant positive correlations between DMS and derived surface NO_3 concentrations, PAR, and chl-*a* are also observed (r=0.30, r=0.41, and r=0.34 respectively). In contrast to other provinces, we observed a statistically significant correlation between DMS and NCP in the CCAL province (r=0.43). The lack of other significant correlations in the province may, in part, reflect the lower number of data points obtained for this region.

Moving beyond simple pairwise correlations, multi-variate empirical algorithms provide an additional approach to assess the potential drivers of regional DMS dynamics. We evaluated the ability of four previously published algorithms to reproduce patterns in the DMS observations. In order to obtain the best possible results, we modified the original equations, using a least squares method to obtain the best-fit coefficients for our data set. We evaluated the algorithm outputs against observations using Pearson's correlation coefficients and root mean square errors (RMSE). As shown in Table 5, model performance was generally low in all cases, with correlation coefficients less than 0.62 and RMSE values ranging from 1.2 to 81.6 nM. No single model performed best in all provinces. For example, while the customized SD02 model was the best performing in the CCAL province (r=0.62, and RMSE=1.6 nM), this model performed poorly elsewhere. The customized VS07 (with coefficients tuned to the NESAP data) showed the best overall performance across the entire NESAP region. Yet, even this model showed only weak correlation between predicted and observed DMS values (r=0.31). Interestingly, the original linear coefficients for this model yielded DMS concentrations that were inversely correlated to the measured values. In no case did models using original linear coefficients outperform those using recalculated coefficients.

4 Discussion

Our results provide new information on the fine-scale and regional patterns of DMS distributions across the NESAP. Our ship-board observations document sub-mesoscale variability in DMS concentration across hydrographic frontal zones, with associated process measurements providing insight into potential driving factors. By combining these new data with more

© Author(s) 2018. CC BY 4.0 License.

than three decades of DMS measurements, we are able to improve data coverage for the NESAP to examine larger-scale spatial patterns and provide a more robust regional climatology to evaluate potential empirical predictive algorithms.

4.1 Contrasting cycling regimes within the NESAP

A number of studies have documented differences in DMS dynamics across oceanographic regimes in the NESAP (Royer et al. 2010, Asher et al. 2011, 2017). These regional differences result from complex ecosystem and environmental interactions, and limit broad-scale prediction of DMS concentrations and sea–air fluxes (Galí et al. 2018). Taxonomic composition of phytoplankton assemblages has been identified as a main driver of DMS distribution patterns. For example, dinoflagellates and prymnesiophytes typically have elevated DMS production, associated with greater intracellular concentrations of DMSP and, in some cases, high activity of DMSP lyase (the enzyme that cleaves DMSP to DMS and acrylate) (Keller 1989; Steinke et al. 2002; Wolfe et al. 2002; Curson et al. 2018). In contrast, bloom-forming diatom species have typically lower intracellular DMSP levels (Keller 1989). However, nutrient limitation has been shown to significantly increase diatom DMS/P production (Bucciarelli and Sunda 2003; Sunda et al. 2007; Harada et al. 2009). Thus, the accumulation of DMS in the water column depends on both the composition of phytoplankton assemblages and their physiological state. Other factors, including zooplankton grazing and the metabolic demands of heterotrophic bacteria are also important (Levasseur et al. 1996, Kiene and Linn 2000, Merzouk et al. 2006, Asher et al. 2017). Below, we discuss the potential factors driving high DMS concentrations along three frontal zones exhibiting sharp DMS concentration gradients. Specifically, we contrast the nanophytoplankton dominated T1 transect with the diatom-dominated coastal T2 and T3 transects, examining the environmental and biological conditions that may have led to the different DMS accumulation patterns in these areas.

4.2 The importance of phytoplankton assemblage composition

The T1 transect, located in the southern-most portion of the ALSK province, spanned 5˚ of longitude from deep (>3000 m) offshore waters, across the shelf break into nearshore waters over the continental shelf. These oceanographic regimes were separated by strong hydrographic frontal features in the vicinity of the shelf break. The negative correlation between DMS and chl-*a* along this transect demonstrates that DMS accumulation did not directly scale with bulk phytoplankton biomass. Rather, our results suggest that DMS concentrations were likely influenced by phytoplankton assemblage composition, with the highest DMS concentrations associated with the greatest relative proportion of prymnesiophytes (Fig. 4c) and the highest DMSPt:chl-*a* (Fig. 4d). Similar relationships have been documented in numerous studies focusing on offshore waters of the NESAP. In these areas, elevated DMS concentrations are often attributed to a preponderance of high-DMSP phytoplankton taxa.

Comparison of T2 and T3 with T1 show that the association of elevated DMS with prymnesiophyte dominance and high DMSPt:chl-*a* ratios did not hold across our entire survey region. As has been observed in previous studies, we measured generally low DMSPt:chl-*a* ratios in the diatom-dominated coastal waters of T2 and T3 (Fig. 6d, 7d). Yet, DMS concentrations

© Author(s) 2018. CC BY 4.0 License.

measured in these waters were extremely high, at times exceeding 20 nM (Fig. 2a). Unlike the T1 transect, DMS concentrations along T2 and T3 increased with decreasing DMSPt:chl-*a* ratios, and were strongly correlated with diatom abundance.

One potential explanation for the difference between T1 and T2/T3 may relate to the different location of these sampling regions. The T1 transect sits along the transition between offshore and inshore water, where different nutrient regimes control phytoplankton productivity. Inshore waters over the continental shelf are typically limited by macronutrients, whereas offshore waters transition into iron-limitation (Boyd and Harrison 1999). At the boundary between these regimes, mixing of water masses through horizontal advection can stimulate phytoplankton productivity (Lam and Letters 2008). Ribalet et al. (2010) observed an active community of nanoplankton in the transitional waters, and attributed this to the stimulation of (often high-DMSP yielding) oceanic phytoplankton by water mass mixing, at the boundary of macro- and micro-nutrient rich waters. Eddy formation and associated transport and mixing may also play a role in stimulating productivity in transition waters (Johnson et al. 2005; Whitney et al. 2005). In support of this, we observed the highest DMS associated with positive SSHA along T1 (Fig. 5).

In contrast to the transition waters, nearshore waters over the continental shelf are typically dominated by low DMSP-producing diatoms. Elevated DMS in these diatom-rich waters may reflect a combination of high absolute biomass and an upregulation of DMSP production observed under nutrient stress (Bucciarelli and Sunda 2003; Sunda et al. 2007; Hockin et al. 2012; Bucciarelli et al. 2013). A meta-analysis by McParland and Levine (in revision) reported an average 12-fold upregulation of intracellular DMSP production under nutrient-stress conditions among phytoplankton typically considered low-producers. By comparison, high DMSP producers only showed an average 1.4-fold upregulation.

In coastal waters, seasonal upwelling may drive high phytoplankton biomass accumulation and increased DMS production in the late-bloom phase, when stratified surface layers are exposed to higher mean light intensities (due to more shallow mixing) and become depleted of nutrients (Zindler et al. 2012). These environmental conditions would act to increase cellular oxidative stress, thus promoting the production of DMS/P as part of a response mechanism (Sunda et al. 2002). The results of Asher et al. (2017) demonstrating high DMS concentrations in post-upwelling waters support this idea. Measurements of SSHA in coastal regions can provide a signature for recent upwelling. The combined effect of wind-induced seasonal water transport offshore and the presence of high density (cold and saline) upwelled water acts to depress sea surface height relative to annual means (Smith 1974; Tabata et al. 1986; Strub and James 1995; Saraceno et al. 2008; Venegas et al. 2008). Negative relationships between DMS concentrations and SSHA were observed in both the T2 and T3 transects, suggesting an association between DMS and upwelling events.

© Author(s) 2018. CC BY 4.0 License.

Additional ecosystem processes may influence DMS accumulation in surface waters. In particular, zooplankton grazing and viral infection may increase DMS concentrations, due to the release of cellular DMSP in phytoplankton during sloppy feeding and cellular lysis. Both of these factors are density-dependent, and thus likely to become more significant with higher phytoplankton cell densities in the late bloom phase. Unfortunately, we do not have measurements to address these processes directly, but the elevated DMSPd concentrations along T3 (~7 nM) may reflect viral and zooplankton mediated loss of particulate DMSP into the dissolved pool.

Taken together, our results support previous studies showing the importance of DMSP-rich species in driving high DMS concentration in offshore waters of the NESAP. In coastal waters, it appears that diatom-dominated phytoplankton assemblages can also support elevated DMS accumulation, particularly under high biomass conditions during the late bloom phase.

4.3 The effect of DMS/P consumption rate on DMS distribution

DMS consumption rates constants across our study area can be translated to biological DMS turnover times ranging from 9 h to 2.5 d (average of 25 h). By comparison, turnover times calculated from sea–air flux removal rates averaged 6.1 d across this area. While these measures do not encompass all loss processes, biological consumption and sea–air flux alone are sufficient to quickly erase a DMS accumulation signature in the mixed layer. Thus, DMS concentrations measured here appear to be reflective of short-term production and consumption processes.

Across our study area, biological DMS removal rate constants (d^{-1}) were inversely related to DMS concentrations (r=-0.55, p=0.03), with lower k_{DMS} in waters with elevated DMS. The relationship may reflect a time-lag of bacterial response to increased DMS concentrations. Results from previous studies have shown that bacterial consumption of DMS increases some time after a rapid rise in DMS, resulting in consumption rate constants that are relatively low when DMS concentrations are initially high. As consumption rate constants increase, DMS concentrations decrease (Zubkov et al. 2004; del Valle et al. 2009). These results, along with the observed positive correlation between DMS and bacterial activity (r=0.53, p=0.03), suggest that microbial consumption is an important control on DMS accumulation, regardless of phytoplankton community assemblage. In contrast to DMS rate constants (d^{-1}), water column DMS consumption rates (nM d^{-1}) showed a positive correlation with DMS concentrations (r=0.65, p=0.01). This result is not unexpected, as consumption rates are the product of rate constants and in situ concentrations. Regardless, the positive correlation between DMS loss rates and concentrations suggests that microbial consumption may not be sufficient to offset new DMS production. Previous studies have examined the impact of DMS loss and production in driving distributions, demonstrating, in some cases, a correlation between DMS concentrations and microbial consumption and production rates (Wolfe and Kiene 1993; Zubkov et al. 2002 Merzouk et al. 2006, Vila-Costa et al. 2008). Our observed relationship between DMS and k_{DMS} and bacterial activity may reflect the

© Author(s) 2018. CC BY 4.0 License.

preponderance of on-shelf stations measured for DMS consumption in our survey (10 out of 16 stations), and significantly higher rates of bacterial metabolism in onshore waters (5.51 ± 2.0 vs 0.73 ± 0.20 nM Leucine uptake d^{-1} for on- and off-shelf stations, respectively). In contrast to biological loss, turnover time due to sea-air flux showed no correlation to DMS concentrations.

Recent studies in the NESAP have estimated that photo-oxidation may account for 20–70 % of gross DMS removal in the NESAP (Asher et al. 2017), and it possible that this process is particularly important in offshore waters. Bouillon and Miller (2004) found that quantum yields of DMS oxidation in the NESAP correlated well to nitrate concentrations, suggesting that this pathway is particularly relevant in the HNLC region where excess macronutrients persist throughout the summer. Thus, the role of biological DMS consumption on influencing total DMS concentrations may be more important in the generally low nitrate coastal waters.

No correlation was found between DMSPd loss rates or loss rate constants and DMS concentrations in our study. This lack of correlation may be due, in part, to variation in DMSPd loss pathways. The DMS yield of DMSP metabolism can vary significantly depending on metabolic needs of bacteria present, and relative abundance of phytoplankton with DMSP lyase activity (Yoch 2002). In the NESAP, a low carbon to organic sulfur ratio in the HNLC regime results in increased DMS-yield from DMSP metabolism, whereas onshore DMS-yield is relatively lower (Merzouk et al. 2006; Royer et al. 2010). Further, variation in DMS loss processes may obscure a relationship between DMSPd cleavage and DMS concentrations, as high loss terms may disproportionately impact net DMS production.

Regardless, correlation between DMSPd and DMS concentrations ($r=0.51$, $p=0.01$) indicate that this compound is likely an important DMS precursor, as widely noted in literature. We are currently investigating, in greater detail, the patterns of DMS and DMSPd consumption from our O16 and O17 cruises (Kiene et al., in prep).

4.4 Insights from merged data set

Our merged data set, binned to 1˚ x 1˚ spatial resolution, builds on the L11 climatology to further constrain summertime DMS distributions across the NESAP region. Despite an overall ~20 % increase in data-containing bins, and the inclusion of data from seven additional years, we see only small changes in the derived climatological DMS concentrations and sea–air fluxes when compared to the PMEL data set used by L11 (Table 3). Our new observations thus support the validity of the L11 climatology in the NESAP region, providing further confidence in the apparent distribution patterns, and a greater spatial footprint for the climatological field. A significant result of our analysis is the presence of high DMS:chl-*a* in offshore waters (Fig. 10c), building on previous reports of higher DMSP:chl-a concentrations in offshore NESAP waters, and highlighting the

© Author(s) 2018. CC BY 4.0 License.

importance of prymnesiophytes and other DMSP-rich phytoplankton taxa in driving DMS accumulation in offshore NESAP waters.

4.5 Biogeochemical provinces

When examining results from our 1° binned data set, a separation of the NESAP into on- and off-shelf regimes does not capture the biogeochemical complexities of the region. Ecological provinces, as defined by Longhurst (2007), define regions with coherent seasonal trends in physical processes, which give rise to similar biological and chemical characteristics. The use of Longhurst's biogeochemical provinces may thus be a more suitable (though still imperfect) approach to examine large-scale and long-term differences in DMS cycling across the region. Work by Reygondeau et al. (2013) has demonstrated the potential for shifts in province boundaries over time, including decrease of coastal province size during El Nino periods, and a general shore-ward shift of ALSK boundaries during summer months. A model-based classification of marine ecosystems in the North Pacific by Gregr and Bodtker (2007) divides our study region into six domains that show little similarity to Longhurst provinces. It is difficult to say which of these classification schemes is most appropriate for examination of DMS dynamics. However, we follow the approach of L11 and others in using Longhurst's provinces to examine regional cycling differences. While we acknowledge these provinces provide only a crude measure of biogeochemical regimes, they remain a best-approximation without delving into more complicated time-resolved ecological province models (Reygondeau et al. 2013). Further, the use of these provinces allowed us to directly compare our results with those of L11. Going forward, it may be useful to examine DMS dynamics in sub-regions defined with a number of different metrics.

4.6 Correlation with environmental variables

Our analysis shows that no single variable can explain an appreciable amount of variability in DMS concentrations across the NESAP. This result is consistent with previous global and regional studies (Kettle et al. 1999; Vézina 2004; Lana et al. 2011). Nonetheless, an examination of the differing relationships between DMS concentrations and other environmental variables provides insight into potential underlying factors driving DMS distribution (Table 4). For example, although we found a moderately strong significant positive correlation between DMS and chl-*a* in the largely HNLC PSAE province, no relationship is observed between these variables in the CCAL province. As noted above and confirmed in several previous studies, the phytoplankton community structure in the offshore PSAE region consists largely of small, DMSP-rich species (Booth et al. 1993; Suzuki et al. 2002; Royer et al. 2010; Steiner et al. 2012), and large blooms are infrequent. Indeed, the average binned chl-*a* concentration in this province is < 1 µg L^{-1}. As such, modest increases chl-*a* likely reflects a stimulation of this high DMSP-producing community. The positive correlation with calcite (an indicator of high-DMSP producing coccolithophores) supports this idea.

The relationship between chl-*a* and DMS is more complicated in the CCAL. High productivity in coastal upwelling zones results in a strong onshore/offshore trend in average chl-*a* concentrations. Yet, no such trend is observed in DMS

© Author(s) 2018. CC BY 4.0 License.

concentrations. This may be due, in part, to the sensitivity of DMS concentrations to phytoplankton assemblage composition and bloom dynamics. High phytoplankton biomass alone will not result in elevated DMS. Rather, elevated DMS concentrations may occur as a response to conditions of late-bloom nutrient stress, as discussed above.

Factors driving observed DMS distribution patterns in the ALSK province are more difficult to surmise. DMS is notably high in the cold, productive waters adjacent to the Alaskan Peninsula. This is affirmed by a weak negative correlation between DMS and SST, and the positive correlation between DMS and chl-*a*. Given that this portion of the province is known to experience localized summer upwelling, it is possible that high DMS in the regions simply reflects elevated productivity.

4.6 Algorithm performance

Our results suggest that no single empirical algorithm is likely to perform well in predicting DMS distributions across the subarctic Pacific. Perhaps the most interesting result was the negative correlation between measured and modeled results using the VS07 algorithm. This algorithm predicts DMS concentrations from solar radiative dose, a term that measures depth-integrated exposure to sunlight, with the assumption that increases in SRD are accompanied by increases in DMS due to UV-induced oxidative stress (Vallina and Simó 2007). However, it is also possible that elevated SRD can also lead to a decrease in surface water DMS concentrations through DMS photo-oxidation. As observed in previous studies, photo-oxidation in the NESAP may account for up to 70 % of gross DMS removal, and rates are positively correlated with nitrate concentrations (Bouillon and Miller 2004; Asher et al. 2017). Thus, in the high-nitrate NESAP, SRD may serve primarily to remove DMS from surface waters, rather than stimulate DMS production. This result, as well as the regionally-varying performance of other tested algorithms, underlines the need for tuning and selecting models best suited for a given area and season. In the absence of a single robust predictive algorithm for DMS concentrations in the NESAP, it will be important to improve mechanistic understanding of DMS/P dynamics, merging field-based process studies with prognostic numerical models (e.g. Aumont et al. 2002, Clainche et al. 2004, Steiner et al. 2012, Wang et al. 2015, Hayashida et al. 2016).

5 Conclusion

This study examines distribution and cycling of DMS across the NESAP at various spatial scales. Our results affirm the importance of high-DMSP producers (i.e. prymnesiophytes) to DMS accumulation in offshore waters, while also demonstrating the importance of diatom-dominated assemblages in driving DMS distribution in coastal upwelling regions. We further highlight the importance of metabolic rate processes and provide evidence for the importance of DMS consumption on concentration gradients at a fine-scale. On the short spatial scales covered by our transect surveys, we observed strong correlations between DMS concentrations and other variables (i.e. SSHA, salinity). Over regional scales, however, we only observed weak statistical relationships. All predictive algorithms we tested showed poor performance in predicting DMS concentrations across the NESAP region, although performance was improved through the use of regionally-tuned coefficients.

© Author(s) 2018. CC BY 4.0 License.

Our compiled data set further support the importance of the NESAP as a global DMS 'hot spot', with patterns of DMS concentrations and sea–air fluxes similar to those observed in Lana et al.'s 2011 climatology. Given the significance of the NESAP in global oceanic DMS emissions, future studies should seek to improve mechanistic understanding of the factors driving DMS accumulation in this region, with the aim of predicting climate-dependent changes over the coming decades.

Code availability

The codes used for spatial binning and data analysis can be provided by the authors upon request.

Data availability

All previously publicly unavailable DMS concentration data presented here have been submitted to the NOAA PMEL database (http://saga.pmel.noaa.gov/dms/). Ancillary shipboard and satellite data can be provided by the authors upon request.

Author contributions

A. Herr compiled and analysed all data presented here, wrote all MATLAB codes, and wrote the manuscript, with editing and intellectual input provided by P. Tortell and R. Kiene. R. Kiene further provided all biological rate measurement data presented here.

Competing interests

The authors declare that they have no conflict of interest.

Acknowledgements

We wish to thank many individuals involved in data collection and logistical aspects of the cruises presented here, including scientists from the Institute of Ocean Sciences, the captain and crew of the R/V *Oceanus* and the CCGS *John P. Tully*, and members Tortell, Kiene, Levine and Hatton laboratory groups. We also thank T. Ahlvin for GIS support. Support for this work was provided from the US National Science Foundation (Grant #1436344), and from the Natural Sciences and Engineering Research Council of Canada.

© Author(s) 2018. CC BY 4.0 License.

References

Asher, E. C., Merzouk, A., and Tortell, P. D.: Fine-scale spatial and temporal variability of surface water dimethylsufide (DMS) concentrations and sea–air fluxes in the NE Subarctic Pacific, Mar. Chem., 126, 63–75, doi:10.1016/j.marchem.2011.03.009, 2011.

Asher, E., Dacey, J. W., Ianson, D., Peña, A., and Tortell, P.D.: Concentrations and cycling of DMS, DMSP, and DMSO in coastal and offshore waters of the Subarctic Pacific during summer, 2010-2011, J. Geophys. Res.-Oceans, 122(4), 3269–3286, doi:10.1002/2016JC012465, 2017.

Aumont, O., Belviso, S., and Monfray, P.: Dimethylsulfoniopropionate (DMSP) and dimethylsulfide (DMS) sea surface distributions simulated from a global three-dimensional ocean carbon cycle model, J. Geophys. Res.-Oceans, 107, 3029, doi:10.1029/1999JC000111, 2002.

Balch, W. M., Gordon, H. R., Bowler, B. C., Drapeau, D. T., and Booth, E. S.: Calcium carbonate measurements in the surface global ocean based on Moderate-Resolution Imaging Spectroradiometer data, J. Geophys. Res.-Oceans, 110, C07001, doi:10.1029/2004JC002560, 2005.

Booth, B., Lewin, J., and Postel, J.: Temporal variation in the structure of autotrophic and heterotrophic communities in the subarctic Pacific, Prog. Oceanogr., 32, 57–99, doi:10.1016/0079-6611(93)90009-3, 1993.

Bouillon, R.-C., and Miller, W. L.: Determination of apparent quantum yield spectra of DMS photo-degradation in an in situ iron-induced Northeast Pacific Ocean bloom, Geophys. Res. Lett., 31, L06310, doi:10.1029/2004GL019536, 2004.

Boyd, P.J. and Harrison, P.J.: Phytoplankton dynamics in the NE subarctic Pacific, Deep-sea Res. Pt. I., 46, 2405–2432, doi:10.1016/S0967-0645(99)00069-7, 1999.

Boyd, P. W., Law, C. S., Wong, C. S., Nojiri, Y., Tsuda, A., Levasseur, M., Takeda, S., Rivkin, R., Harrison, P. J., Strzepek, R., Gower, J., McKay, M., Abraham, E., Arychuk, M., Barwell-Clarke, J., Crawford, W., Crawford, D., Hale, M., Harada, K., Johnson, K., Kiyosawa, H., Kudo, I., Marchetti, A., Miller, W., Needoba, J., Nishioka, J., Ogawa, H., Page, J., Robert, M., Saito, H., Sastri, A., Sherry, N., Soutar, T., Sutherland, N., Taira, Y., Whitney, F., Wong, S.-K. E., and Yoshimura, T.: The decline and fate of an iron-induced subarctic phytoplankton bloom, Nature 428, 549–553, doi:10.1038/nature02412, 2004.

© Author(s) 2018. CC BY 4.0 License.

Brewin, R., Sathyendranath, S., Hirata, T., Lavender, S., Barciela, R., and Hardman-Mountford, N.: A three-component model of phytoplankton size class for the Atlantic Ocean, Ecol. Model., 221, 1472–1483, doi:10.1016/j.ecolmodel.2010.02.014, 2010.

Bricaud, A., Babin, M., Morel, A. and Claustre, H.: Variability in the chlorophyll-specific absorption coefficients of natural phytoplankton: Analysis and parameterization, J. Geophys. Res.-Oceans, 100, 13321–13332, doi:10.1029/95JC00463, 1995.

Bucciarelli, E., and Sunda, W.: Influence of CO2, nitrate, phosphate, and silicate limitation on intracellular dimethylsulfoniopropionate in batch cultures of the coastal diatom Thalassiosira pseudonana, Limnol. Oceanogr., 48, 2256–2265, doi:10.4319/lo.2003.48.6.2256, 2003.

Bucciarelli, E., Ridame, C., Sunda, W., Dimier-Hugueney, C., Cheize, M., and Belviso, S.: Increased intracellular concentrations of DMSP and DMSO in iron-limited oceanic phytoplankton Thalassiosira oceanica and Trichodesmium erythraeum, Limnol. Oceanogr., 58, 1667–1679, doi:10.4319/lo.2013.58.5.1667, 2013.

Burt, W., Westberry, T., Behrenfeld, M., Zeng, C., Izett, R., Tortell, P.: Carbon: Chlorophyll Ratios and Net Primary Productivity of Subarctic Pacific Surface Waters Derived From Autonomous Shipboard Sensors, Global Biogeochem. Cy., 32, 267–288, doi:10.1002/2017GB005783, 2018.

Charlson, R. J., Lovelock, J. E., Andreae, M. O. and Warren, S. G.: Oceanic phytoplankton, atmospheric sulphur, cloud albedo and climate, Nature, 326, 655–661, doi:10.1038/326655a0, 1987.

Clainche, Y. L., Levasseur, M., Vézina, A., Dacey, J. W. H., and Saucier, F. J.: Behaviour of the ocean DMS (P) pools in the Sargasso Sea viewed in a coupled physical-biogeochemical ocean model, Can. J. Fish. Aquat. Sci., 61, 788–803, doi:10.1139/F04-027, 2004.

Crawford, W., Brickley, P., Peterson, T., and Thomas, A.: Impact of Haida Eddies on chlorophyll distribution in the Eastern Gulf of Alaska, Deep-Sea Res. Pt. II, 52, 975–989, doi:10.1016/j.dsr2.2005.02.011, 2005.

Curson, A., Williams, B., Pinchbeck, B., Sims, L., Martínez, A., Rivera, P., Kumaresan, D., Mercadé E., Spurgin, L., Carrión O., Moxon S., Cattolico, R., Kuzhiumparambil, U., Guagliardo, P., Clode, P., Raina, J.-B., and Todd, J.: DSYB catalyses the key step of dimethylsulfoniopropionate biosynthesis in many phytoplankton, Nat. Microbiol., 3, 430–439, doi:10.1038/s41564-018-0119-5, 2018.

© Author(s) 2018. CC BY 4.0 License.

Dacey, J. W., and Blough, N. V.: Hydroxide decomposition of dimethylsulfoniopropionate to form dimethylsulfide, Geophys. Res. Lett., 14, 1246–1249, doi:10.1029/GL014i012p01246, 1987.

Franklin, D. J., Poulton, A. J., Steinke, M., Young, J., Peeken, I., and Malin, G.: Dimethylsulphide, DMSP-lyase activity and microplankton community structure inside and outside of the Mauritanian upwelling, Prog. Oceanogr., 83, 134–142, doi:10.1016/j.pocean.2009.07.011, 2009.

Galí, M., Levasseur, M., Devred, E., Simó, R., and Babin, M.: Sea-surface dimethylsulfide (DMS) concentration from satellite data at global and regional scales, Biogeosciences, 15, 3497–3519, doi:10.5194/bg-2018-18, 2018.

Goes, J., Saino, T., Oaku, H., Ishizaka, J., Wong, C., and Nojiri, Y: Basin scale estimates of sea surface nitrate and new production from remotely sensed sea surface temperature and chlorophyll, Geophys. Res. Lett., 27, 1263–1266, doi:10.1029/1999GL002353, 2000.

Gordon, H. R., Boynton, G. C., Balch, W. M., Groom, S. B., Harbour, D. S., and Smyth, T. J.: Retrieval of coccolithophore calcite concentration from SeaWiFS imagery, Geophys. Res. Lett., 28, 1587–1590, doi:10.1029/2000GL012025, 2001.

Gregr, E., and Bodtker, K.: Adaptive classification of marine ecosystems: Identifying biologically meaningful regions in the marine environment, Deep-Sea Res. Pt. I, 54, 385–402, doi:10.1016/j.dsr.2006.11.004, 2007.

Harada, H., Vila-Costa, M., Cebrian, J., and Kiene, R.: Effects of UV radiation and nitrate limitation on the production of biogenic sulfur compounds by marine phytoplankton, Aquat. Bot., 90, 37–42, doi:10.1016/j.aquabot.2008.05.004, 2009.

Hatton, A. D., Turner, S. M., Malin, G., and Liss, P. S.: Dimethylsulphoxide and other biogenic sulphur compounds in the Galapagos Plume, Deep-Sea Res. Pt. II, 45, 1043–1053, doi:10.1016/S0967-0645(98)00017-4, 1998.

Hayashida, H., Steiner, N., Monohan, A., Galindo, V., Lizotte, M., and Levasseur, M.: Implications of sea-ice biogeochemistry for oceanic production and emissions of dimethyl sulfide in the Arctic, Biogeosciences, 14, 3129–3155, 2017..

Hirata, T., Aiken, J., Hardman-Mountford, N., Smyth, T. J., and Barlow, R. G.: An absorption model to determine phytoplankton size classes from satellite ocean colour, Remote Sens. Environ., 112, 3153–3159, doi:10.1016/j.rse.2008.03.011, 2008.

© Author(s) 2018. CC BY 4.0 License.

Hirata, T., Hardman-Mountford, N. J., Brewin, R. J., Aiken, J., Barlow, R., Suzuki, K., Isada, T., Howell, E., Hashioka, T., Noguchi-Aita, M., and Yamanaka, Y.: Synoptic relationships between surface Chlorophyll-a and diagnostic pigments specific to phytoplankton functional types, Biogeosciences, 8, 311–327, doi:10.5194/bg-8-311-2011, 2011.

Hockin, N. L., Mock, T., Mulholland, F., Kopriva, S., and Malin, G.: The response of diatom central carbon metabolism to nitrogen starvation is different from that of green algae and higher plants, Plant Physiol., 158, 299–312, doi:10.1104/pp.111.184333, 2012.

Izett, R. W., Manning, C. C., Hamme, R. C., and Tortell, P. D.: Refined Estimates of Net Community Production in the Subarctic Northeast Pacific Derived From ΔO2/Ar Measurements With N2O-Based Corrections for Vertical Mixing, Global Biogeochem. Cy., 32, 326–350, doi:10.1002/2017GB005792, 2018.

Jarníková, T., Dacey, J., Lizotte, M., Levasseur, M., and Tortell, P.: The distribution of methylated sulfur compounds, DMS and DMSP, in Canadian subarctic and Arctic marine waters during summer 2015, Biogeosciences, 15, 2449–2465, doi:10.5194/bg-15-2449-2018, 2018.

Johnson, K., Miller, L., Sutherland, N., and Wong, C. S.: Iron transport by mesoscale Haida eddies in the Gulf of Alaska, Deep-Sea Res. Pt. II, 52, 933–953, doi:10.1016/j.dsr2.2004.08.017, 2005.

Johnson, W., Soule, M., and Kujawinski, E.: Evidence for quorum sensing and differential metabolite production by a marine bacterium in response to DMSP, ISME J., 10, 2304–2316, doi:10.1038/ismej.2016.6, 2016.

Kaiser, J., Reuer, M. K., Barnett, B., and Bender, M. L.: Marine productivity estimates from continuous O2/Ar ratio measurements by membrane inlet mass spectrometry, Geophys. Res. Lett., 32, L19605, doi:10.1029/2005GL023459, 2005.

Keller, M. D.: Dimethyl Sulfide Production and Marine Phytoplankton: The Importance of Species Composition and Cell Size, Biol. Oceanogr., 6, 375–382, doi:10.1080/01965581.1988.10749540, 1989.

Kettle, A. J., Andreae, M. O., Amouroux, D., Andreae, T. W., Bates, T. S., Berresheim, H., Bingemer, H., Boniforti, R., Curran, M. A., DiTullio, G. R., Helas, G., Jones, G. B., Keller, M. D., Kiene, R. P., Leck, C., Levasseur, M., Malin, G., Maspero, M., Matrai, P., McTaggart, A. R., Mihalopoulos, N., Nguyen, B. C., Novo, A., Putaud, J. P., Rapsomanikis, S., Roberts, G., Schebeske, G., Sharma S., Simó, R., Staubes, R., Turner, S., and Uher, G.: A global database of sea surface dimethylsulfide (DMS) measurements and a procedure to predict sea surface DMS as a function of latitude, longitude, and month, Global Biogeochem. Cy., 13, 399–444, doi:10.1029/1999GB900004, 1999.

© Author(s) 2018. CC BY 4.0 License.

Kiene, R. P., and Linn, L. J.: Distribution and turnover of dissolved DMSP and its relationship with bacterial production and dimethylsulfide in the Gulf of Mexico, Limnol. Oceanogr., 45, 849–861, doi:10.4319/lo.2000.45.4.0849, 2000.

Kiene, R. P., and Slezak, D.: Low dissolved DMSP concentrations in seawater revealed by small-volume gravity filtration and dialysis sampling, Limnol. Oceanogr.-Meth., 4, 80–95, doi:10.4319/lom.2006.4.80, 2006.

Kiene, R., and Service, S.: Decomposition of dissolved DMSP and DMS in estuarine waters: dependence on temperature and substrate concentration., Mar. Ecol. Prog. Ser., 76, 1–11, doi:10.3354/meps076001, 1991.

Kiene, R. P., Linn, L. J., and Bruton, J. A.: New and important roles for DMSP in marine microbial communities, J. Sea. Res., 43, 209–224, doi:10.1016/S1385-1101(00)00023-X, 2000.

Lam, P. J., and Letters, J.K.: The continental margin is a key source of iron to the HNLC North Pacific Ocean, Geophys. Res. Lett., 35, L07608, doi:10.1029/2008GL033294, 2008.

Lana, A., Bell, T. G., Simó, R., Vallina, S. M., Ballabrera-Poy, J., Kettle, A. J., Dachs, J., Bopp, L., Saltzman, E. S., Stefels, J., Johnson, J. E., and Liss, P. S.: An updated climatology of surface dimethlysulfide concentrations and emission fluxes in the global ocean, Global Biogeochem. Cy., 25, GB1004, doi:10.1029/2010GB003850, 2011.

Levasseur, M., Michaud, S., Egge, J., Cantin, G., Nejstgaard, J. C., Sanders, R., Fernandez, E., Solberg, P. T., Heimdal, B., and Gosselin, M.: Production of DMSP and DMS during a mesocosm study of an Emiliania huxleyi bloom: influence of bacteria and Calanus finmarchicus grazing, Mar. Biol., 126, 609–618, doi:10.1007/BF00351328, 1996.

Levasseur, M., Scarratt, M. G., Michaud, S., Merzouk, A., Wong, C., Arychuk, M., Richardson, W., Rivkin, R. B., Hale, M., Wong, E., Marchetti, A., and Kiyosawa, H.: DMSP and DMS dynamics during a mesoscale iron fertilization experiment in the Northeast Pacific—Part I: Temporal and vertical distributions, Deep-Sea Res., Pt. II 53, 2353–2369, doi:10.1016/j.dsr2.2006.05.023, 2006.

Li, H., Liu, Z., Xu, J., Wu, X., Chaohui, S., Lu, S., and Minjie, C.: Manual of Global Ocean Argo gridded data set (BOA-Argo) (Version 2017), 2017.

Locarnini, S., Turner, S. and Liss, P.: The distribution of dimethylsulfide, DMS, and dimethylsulfoniopropionate, DSMP, in waters off the Western Coast of Ireland, Cont. Shelf Res., 18, 1455–1473, doi:10.1016/S0278-4343(98)00035-1, 1998.

© Author(s) 2018. CC BY 4.0 License.

Longhurst, A. R.: Ecological Geography of the Sea, 2nd ed. Elsevier, doi:10.1016/B978-0-12-455521-1.X5000-1, 2007.

Lovelock, J., Maggs, R., and Rasmussen, R.: Atmospheric dimethyl sulphide and the natural sulphur cycle, Nature, 237, 452–453, doi:10.1038/237452a0. 1972.

McParland, E. and Levine, N.: The role of differential DMSP regulation and community composition in predicting variability of global surface DMSP concentrations, Limnol. Oceanogr., in revision.

Merzouk, A., Levasseur, M., Scarratt, M. G., Michaud, S., Rivkin, R. B., Hale, M. S., Kiene, R. P., Price, N. M., and Li, W.: DMSP and DMS dynamics during a mesoscale iron fertilization experiment in the Northeast Pacific–Part II: Biological cycling, Deep-Sea Res. Pt. II, 53, 2370–2383, doi:10.1016/j.dsr2.2006.05.022, 2006.

Nemcek, N., Ianson, D., and Tortell, P.: A high-resolution survey of DMS, CO2, and O2/Ar distributions in productive coastal waters, Global Biogeochem. Cy., 22, GB2009, doi:10.1029/2006GB002879, 2008.

Reisch, C. R., Stoudemayer, M. J., Varaljay, V. A., Amster, I. J., Moran, M. A., and Whitman, W.: Novel pathway for assimilation of dimethylsulphoniopropionate widespread in marine bacteria, Nature, 473, 208–211, doi:10.1038/nature10078, 2011.

Reuer, M., Barnett, B., Bender, M., Falkowski, P., and Hendricks, M.: New estimates of Southern Ocean biological production rates from O2/Ar ratios and the triple isotope composition of O2, Deep-Sea Res. Pt. I, 54, 951–974, doi:10.1016/j.dsr.2007.02.007, 2007.

Reygondeau, G., Longhurst, A., Martinez, E., Beaugrand, G., Antoine, D., and Maury, O.: Dynamic biogeochemical provinces in the global ocean, Global Biogeochem. Cy., 27, 1046–1058, doi:10.1002/gbc.20089, 2013.

Ribalet, F., Marchetti, A., Hubbard, K., Brown, K., Durkin, C., Morales, R., Robert, M., Swalwell, J., Tortell, P., and Armbrust, V.: Unveiling a phytoplankton hotspot at a narrow boundary between coastal and offshore waters, P. Natl. A. Sci. USA, 107, 16571–16576, doi:10.1073/pnas.1005638107, 2010.

Roesler, C., and Barnard, A.: Optical proxy for phytoplankton biomass in the absence of photophysiology: Rethinking the absorption line height, Methods in Oceanography, 7, 79–94, doi:10.1016/j.mio.2013.12.003, 2013.

© Author(s) 2018. CC BY 4.0 License.

Royer, S.-J., Levasseur, M., Lizotte, M., Arychuk, M., Scarratt, M., Wong, C., Lovejoy, C., Robert, M., Johnson, K., Peña, A., Michaud, S., and Kiene, R.:. Microbial dimethylsulfoniopropionate (DMSP) dynamics along a natural iron gradient in the northeast subarctic Pacific, Limnol. Oceanogr., 55, 1614–1626, doi:10.4319/lo.2010.55.4.1614, 2010.

Saltzman, E. S., King, D. B., Holmen, K., and Leck, C.: Experimental determination of the diffusion coefficient of dimethylsulfide in water, J. Geophys. Res., 98, 16481–16468, doi:10.1029/93JC01858, 1993.

Saraceno, M., Strub, P. T., and Kosro, P. M.: Estimates of sea surface height and near-surface alongshore coastal currents from combinations of altimeters and tide gauges, J. Geophys. Res.-Oceans, 113, C11013, doi:10.1029/2008JC004756, 2008.

Schuback, N., Schallenberg, C., Duckham, C., Maldonado, M. and Tortell, P.: Interacting Effects of Light and Iron Availability on the Coupling of Photosynthetic Electron Transport and CO2-Assimilation in Marine Phytoplankton, Plos One, 10: e0133235, doi:10.1371/journal.pone.0133235, 2015.

Seymour, J. R., Simó, R., Ahmed, T., and Stocker, R.: Chemoattraction to Dimethylsulfoniopropionate Throughout the Marine Microbial Food Web, Science, 329, 342–345, doi:10.1126/science.1188418, 2010.

Simó, R.: From cells to globe: approaching the dynamics of DMS (P) in the ocean at multiple scales, Can. J. Fish. Aquat. Sci., 61, 673–684, doi:10.1139/f04-030, 2004.

Simó, R., and Dachs, J.: Global ocean emission of dimethylsulfide predicted from biogeophysical data, Global Biogeochem. Cy., 16, 1078, doi:10.1029/2001GB001829, 2002.

Smith, D., and Azam, F.: A simple, economical method for measuring bacterial protein synthesis rates in seawater using 3H-leucine, Marine Microbial Food Webs, 6, 107–114, 1992.

Smith, R. L.: A description of current, wind, and sea level variations during coastal upwelling off the Oregon coast, July–August 1972, J. Geophys. Res., 79, doi:10.1029/JC079i003p00435, 1974.

Stefels, J., Steinke, M., Turner, S., Malin, G., and Belviso, S.: Environmental constraints on the production and removal of the climatically active gas dimethylsulphide (DMS) and implications for ecosystem modelling, Biogeochemistry, 83, 245–275, doi:10.1007/s10533-007-9091-5, 2007.

© Author(s) 2018. CC BY 4.0 License.

Steiner, N., Robert, M., Arychuk, M., Levasseur, M., Merzouk, A., Peña, A., Richardson, W. and Tortell, P.: Evaluating DMS measurements and model results in the Northeast subarctic Pacific from 1996–2010, Biogeochemistry, 110, 269–285, doi:10.1007/s10533-011-9669-9, 2012.

Steinke, M., Malin, G., Archer, S. D., Burkill, P. H., and Liss, P. S.: DMS production in a coccolithophorid bloom: evidence for the importance of dinoflagellate DMSP lyases, Aquat. Microb. Ecol., 26, 259–270, doi:10.3354/ame026259, 2002.

Strub, T., and James, C.: The large-scale summer circulation of the California Current, Geophys. Res. Lett., 22, 207–210, doi:10.1029/94GL03011, 1995.

Sunda, W., Kieber, D. J., Kiene, R. P., and Huntsman, S.: An antioxidant function for DMSP and DMS in marine algae, Nature, 418, 317-320, doi:10.1038/nature00851, 2002.

Sunda, W., Hardison, R., Kiene, R., and Bucciarelli, E.: The effect of nitrogen limitation on cellular DMSP and DMS release in marine phytoplankton: climate feedback implications, Aquat. Sci., 69, 341–351, doi:10.1007/s00027-007-0887-0, 2007.

Suzuki, K., Minami, C. , Liu, H., and Saino, T.: Temporal and spatial patterns of chemotaxonomic algal pigments in the subarctic Pacific and the Bering Sea during the early summer of 1999, Deep-Sea Res. Part II, 49, 5685–5704, doi:10.1016/s0967-0645(02)00218-7, 2002.

Sweeney, C., Gloor, E., Jacobson, A. R., Key, R. M., McKinley, G., Sarmiento, J. L., and Wanninkhof, R.: Constraining global air-sea gas exchange for CO2 with recent bomb 14C measurements, Global Biogeochem. Cy., 21, GB2015, doi:10.1029/2006gb002784, 2007.

Tabata, S., Thomas, B. and Ramsden, D.: Annual and interannual variability of steric sea level along line P in the northeast Pacific Ocean, J. Phys. Oceanogr, 16, 1378–1398, doi:10.1175/1520-0485(1986)016<1378:AAIVOS>2.0.CO;2, 1986.

Tortell, P. D.: Dissolved gas measurements in oceanic waters made by membrane inlet mass spectrometry, Limnol. Oceanogr.-Meth., 3, 24–37, doi:10.4319/lom.2005.3.24, 2005a.

Tortell, P. D.: Small-scale heterogeneity of dissolved gas concentrations in marine continental shelf waters, Geochem. Geophy. Geosy., 6, Q11M04, doi:10.1029/2005GC000953, 2005b.

© Author(s) 2018. CC BY 4.0 License.

Uitz, J., Claustre, H., Morel, A., and Hooker, S. B.: Vertical distribution of phytoplankton communities in open ocean: An assessment based on surface chlorophyll, J. Geophys. Res.-Oceans, 111, C08005, doi:10.1029/2005JC003207, 2006.

Del Valle, D. A., Kieber, D. J., Toole, D. A., Brinkley, J., and Kiene, R. P.: Biological consumption of dimethylsulfide (DMS) and its importance in DMS dynamics in the Ross Sea, Antarctica, Limnol. Oceanogr., 54, 785–798, doi:10.4319/lo.2009.54.3.0785, 2009.

Vallina, S., and Simó, R.: Strong relationship between DMS and the solar radiation dose over the global surface ocean, Science 315, 506–508, doi:10.1126/science.1133680, 2007.

Venegas, R. M., Strub, P. T., Beier, E., Letelier, R., Thomas, A. C., Cowles, T., James, C., Soto-Mardones, L., and Cabrera, C.: Satellite-derived variability in chlorophyll, wind stress, sea surface height, and temperature in the northern California Current System, J. Geophys. Res.-Oceans 113, C03015, doi:10.1029/2007JC004481, 2008.

Vézina, A.: Ecosystem modelling of the cycling of marine dimethylsulfide: a review of current approaches and of the potential for extrapolation to global scales, Can. J. Fish. Aquat. Sci., 61, 845–856, doi:10.1139/f04-025, 2004.

Vidussi, F., Claustre, H., Manca, B. B., Luchetta, A., and Marty, J.-C.: Phytoplankton pigment distribution in relation to upper thermocline circulation in the eastern Mediterranean Sea during winter, J. Geophys. Res.-Oceans, 106, doi:10.1029/1999JC000308, 19939–19956, 2001.

Vila-Costa, M., Kiene, R., and Simó, R.: Seasonal variability of the dynamics of dimethylated sulfur compounds in a coastal northwest Mediterranean site, Limnol. Oceanogr., 53, doi:10.4319/lo.2008.53.1.0198, 198–211, 2008.

Wang, S., Elliott, S., Maltrud, M., and Cameron-Smith, P.: Influence of explicit Phaeocystis parameterizations on the global distribution of marine dimethyl sulfide, J. of Geophys. Res.-Biogeo., 120, 2158–2177, doi:10.1002/2015JG003017, 2015.

Watanabe, Y. W., Yoshinari, H., Sakamoto, A., Nakano, Y., Kasamatsu, N., Midorikawa, T. and Ono, T.: Reconstruction of sea surface dimethylsulfide in the North Pacific during 1970s to 2000s, Mar. Chem., 103, 347–358, doi:10.1016/j.marchem.2006.10.004, 2007.

Werdell, J., and Bailey, S.: An improved in-situ bio-optical data set for ocean color algorithm development and satellite data product validation, Remote Sens. Environ., 98, 122–140, doi:10.1016/j.rse.2005.07.001, 2005.

© Author(s) 2018. CC BY 4.0 License.

Whitney, F. A., Crawford, W. R., and Harrison, P. J.: Physical processes that enhance nutrient transport and primary productivity in the coastal and open ocean of the subarctic NE Pacific, Deep-Sea Res. Pt. II, 52, 681–706, doi:10.1016/j.dsr2.2004.12.023, 2005.

Wolfe, G. V., and Kiene, R.P.: Radioisotope and chemical inhibitor measurements of dimethyl sulfide consumption rates and kinetics in estuarine waters, Mar. Ecol. Prog. Ser., 99, 261–269, doi:10.3354/meps099261, 1993.

Wolfe, G. V., Strom, S. L., Holmes, J. L., Radzio, T. and Olson, B. M.: Dimethylsulfiopropionate cleavage by marine phytoplankton in response to mechanical, chemical, or dark stress, J. Phycol., 38, 948–960, doi:10.1046/j.1529-8817.2002.t01-1-01100.x, 2002.

Wong, C., Wong, S., Richardson, W., Ith, G., Arychuk, M., and Page, J. Temporal and spatial distribution of dimethylsulfide in the subarctic northeast Pacific Ocean: a high-nutrient–low-chlorophyll region, Tellus 57B, 317–331, doi:10.1111/j.1600-0889.2005.00156.x, 2005.

Wu, X., Li, P., Liu, C., Zhang, H., Yang, G., Zhang, S., and Zhu, M.: Biogeochemistry of Dimethylsulfide, Dimethylsulfoniopropionate, and Acrylic Acid in the Changjiang Estuary and the East China Sea, J. Geophys. Res.-Oceans, 122, 10,245–10,261, doi:10.1002/2017JC013265, 2017.

Yoch, D. C.: Dimethylsulfoniopropionate: its sources, role in the marine food web, and biological degradation to dimethylsulfide, Appl. Environ. Microbiol., 68, 5804–5815, doi:10.1128/AEM.68.12.5804-5815.2002, 2002.

Zeng, C., Rosengard, S. Z., Burt, W., Peña, A., Nemcek, N., Zeng, T., Arrigo, K. R., and Tortell, P. D.: Optically-derived estimates of phytoplankton size class and taxonomic group biomass in the Eastern Subarctic Pacific Ocean, Deep-Sea Res. Pt. I, 136, 107–118, doi:10.1016/j.dsr.2018.04.001, 2018.

Zindler, C., Peeken, I., and Marandino, C.: Environmental control on the variability of DMS and DMSP in the Mauritanian upwelling region, Biogeosciences, 9, 1041–1051, doi:10.5194/bg-9-1041-2012, 2012.

Zubkov, M. V., Fuchs, B. M., Archer, S. D., and Kiene, R. P.: Rapid turnover of dissolved DMS and DMSP by defined bacterioplankton communities in the stratified euphotic zone of the North Sea, Deep-Sea Res. Pt. II, 49, 3017–3038, doi:10.1016/S0967-0645(02)00069-3, 2002.

Zubkov, M., Linn, L. J., Amann, R., and Kiene, R. P. Temporal patterns of biological dimethylsulfide (DMS) consumption during laboratory-induced phytoplankton bloom cycles, Mar. Ecol. Prog. Ser., 271, 77–86, doi:10.3354/meps271077, 2004.

Biogeosciences Discuss., https://doi.org/10.5194/bg-2018-411
Manuscript under review for journal Biogeosciences
Discussion started: 11 October 2018
© Author(s) 2018. CC BY 4.0 License.

Table 1. Summary of DMS data included in this study. With the exception of the PMEL data, all measurements are derived from membrane inlet mass spectrometry (MIMS).

Cruise abbreviation	Vessel affiliation; cruise name and number	Sampling dates	Areal extent	Provinces included	No. data points	References
VIJ04	DFO; Central Coast BioChemical Study; 2004-24	12–19 Aug 2004	48° N - 52° N 131 ° W - 123° W	ALSK, CCAL	1913	(Nemcek et al. 2008)
LPJ07	DFO; Line P; 2007-13	1–16 Jun 2007	47° N - 55° N 146 ° W - 123° W	ALSK, CCAL, PSAE	21478	(Asher et al. 2011)
LPA07	DFO; Line P; 2007-15	16–30 Jun 2007	48° N - 54° N 146 ° W - 123° W	ALSK, CCAL, PSAE	16418	(Asher et al. 2011)
LPJ08	DFO; Line P; 2008-26	1–15 Jun 2008	48°N - 52°N 146 ° W - 123° W	ALSK, CCAL, PSAE	15304	(Asher et al. 2011)
LPA08	DFO; Line P; 2008-27	14–30 Aug 2008	48°N - 52°N 146 ° W - 123° W	ALSK, CCAL, PSAE	20881	(Asher et al. 2011)
VIJ10	DFO; La Perouse; 2010-12	1–4 Jun 2010	48°N - 52°N 130 ° W - 123° W	ALSK, CCAL	4551	(Tortell et al. 2012)
WCAC10	DFO; Ocean Acidification; 2010-36	22 Jul–15 Aug 2010	47°N - 57°N 138 ° W - 123° W	ALSK, CCAL, PSAE	25167	(Asher et al. 2017)
LPA11	DFO; Line P; 2011-27	19–28 Aug 2011	48° N - 51° N 146 ° W - 126° W	CCAL, PSAE	10802	(Asher et al. 2017)
LPA14	DFO; Line P and Strait of Georgia; 2014-19	29–31 Aug 2014	50° N - 51° N 145° W - 134° W	PSAE	2560	(Asher et al. 2015)
O16	UNOLS; Resolving DMS 1: OC-1607A	12–27 Jul 2016	45° N - 56° N 143 ° W - 124° W	ALSK, CCAL, PSAE	18712	Previously unpublished
O17	UNOLS; Resolving DMS II: OC-1708A	12–27 Aug 2017	47° N - 57° N 146 ° W - 126° W	ALSK, CCAL, PSAE	10015	Previously unpublished
PMEL	various	various, 1984–2004	45° N - 61° N 167 ° W - 124° W	ALSK, CCAL, PSAE	3236	Various

Biogeosciences Discuss., https://doi.org/10.5194/bg-2018-411
Manuscript under review for journal Biogeosciences
Discussion started: 11 October 2018
© Author(s) 2018. CC BY 4.0 License.

Table 2. Summertime DMS data coverage across the NESAP region and within Longhurst provinces. Values indicate the number of data-containing 1° x 1° spatial bins out of the total number of bins within the given area. The left column represents the coverage for the PMEL data set (as utilized by L11) and the right column represents the updated data set containing both PMEL measurements and MIM-based DMS concentration measurements.

5

Province Name	PMEL	This Study
CCAL	30/75 (40.0 %)	45/75 (60.0 %)
ALSK	61/119 (51.3 %)	83/119 (69.8 %)
PSAE	5/430 (12.8 %)	114/430 (26.5 %)
Total	126/1140 (11.1 %)	216/1140 (19.0 %)

Biogeosciences Discuss., https://doi.org/10.5194/bg-2018-411
Manuscript under review for journal Biogeosciences
Discussion started: 11 October 2018
© Author(s) 2018. CC BY 4.0 License.

Table 3. Mean DMS concentrations, sea-air fluxes and total summertime DMS flux for the PMEL data set utilized by L11, and the updated data based used in this study.

	PMEL			This Study		
Province Name	DMS (nM)	DMS Flux (µmol m^{-2} d^{-1})	Total summer DMS flux (Tg S)	DMS (nM)	DMS Flux (µmol m^{-2} d^{-1})	Total summer DMS flux (Tg S)
CCAL	4.0 ± 0.5	4.4 ± 0.95	0.01	4.6 ± 0.4	6.3 ± 0.7	0.02
ALSK	8.9 ± 1.1	16.4 ± 4.0	0.06	7.5 ± 0.9	14.4 ± 3.0	0.05
PSAE	8.9 ± 0.7	21.0 ± 4.0	0.38	6.5 ± 0.4	16.5 ± 2.2	0.30
Total	7.2 ± 0.5	12.7 ± 2.0	0.32	6.2 ± 0.3	12.2 ± 1.4	0.30

Biogeosciences Discuss., https://doi.org/10.5194/bg-2018-411
Manuscript under review for journal Biogeosciences
Discussion started: 11 October 2018
© Author(s) 2018. CC BY 4.0 License.

Table 4. Pearson's correlation coefficients between DMS concentrations and other oceanographic variables binned to 1° spatial resolution. DMS data were derived from our combined PMEL and MIMS data set, variables derived from in-situ and satellite-based data. N represents the number of data pairs available for each correlation calculation. * indicates significance of p<0.05.

Variable	Whole region	CCAl	ALSK	PSAE
Salinity	r = -0.04	r = 0.24	r = -0.04	r = 0.07
	N = 223	N = 31	N = 83	N = 102
SST	r = -0.01	r = -0.17	r = -0.32*	r = 0.18
	N =248	N = 44	N = 83	N = 114
Chlorophyll-*a*	r = 0.17*	r = -0.11	r = 0.34*	r = 0.45*
	N =207	N = 31	N = 79	N = 99
Calcite	r = 0.12	r = -0.08	r = -0.01	r = 0.50*
	N =205	N = 30	N = 83	N = 99
PAR	r = 0.04	r = -0.28	r = 0.41*	r = 0.19
	N = 212	N = 32	N =52	N = 91
Depth	r = -0.05	r = 0.20	r = -0.34*	r = -0.02
	N = 201	N = 45	N = 12	N = 96
MLD	r = -0.14	r = 0.14	r = -0.06	r = -0.18
	N = 98	N = 21	N = 11	N = 70
SSN	r = 0.01	r = 0.14	r = 0.30*	r = -0.18
	N = 207	N = 31	N = 79	N = 99
SSHA	r = -0.20*	r = -0.34	r = -0.05	r = -0.47*
	N = 207	N = 30	N = 80	N = 102
NCP	r = 0.22*	r = 0.43*	r = 0.05	r = 0.29
	N = 91	N = 26	N = 25	N = 37
Wind	r = 0.17*	r = -0.06	r = 0.08	r = 0.29*
	N = 249	N = 45	N = 83	N = 114

Biogeosciences Discuss., https://doi.org/10.5194/bg-2018-411
Manuscript under review for journal Biogeosciences
Discussion started: 11 October 2018
© Author(s) 2018. CC BY 4.0 License.

Table 5. Pearson correlation coefficients and root mean square errors (nmol L^{-1}) between observed DMS concentrations and empirical predictions derived from the SD02, VS07 and W07 algorithms, using both published coefficients (original) and coefficients derived specifically for our NESAP observations using a least-squares approach (custom). Algorithm performance is shown for full NESAP region, as well as the three Longhurst biogeographical provinces within our study area. * indicates significance of p<0.05.

Province	SD02 original	SD02 custom	VS07 original	VS07 custom	W07 original	W07 custom
Whole	r = 0.05	r = 0.08	r = -0.31*	r = 0.31*	r = -0.08	r = 0.17*
region	RMSE = 3.77	RMSE = 3.03	RMSE = 4.95	RMSE = 2.63	RMSE = 67.1	RMSE = 5.86
CCAL	r = 0.04	r = 0.62*	r = -0.23	r = 0.23	r = -0.17	r = 0.27
	RMSE = 3.42	RMSE = 1.61	RMSE = 4.54	RMSE = 1.20	RMSE = 81.6	RMSE = 2.04
ALSK	r = 0.16	r = 0.12	r = -0.10	r = 0.10	r = -0.20	r = 0.53*
	RMSE = 2.37	RMSE = 2.07	RMSE = 3.43	RMSE = 2.09	RMSE = 47.5	RMSE = 7.19
PSAE	r = 0.09	r = 0.23	r = -0.39*	r = 0.39*	r = -0.01	r = 0.44*
	RMSE = 3.97	RMSE = 2.94	RMSE = 5.28	RMSE = 2.81	RMSE = 20.6	RMSE = 4.59

5

Biogeosciences Discuss., https://doi.org/10.5194/bg-2018-411
Manuscript under review for journal Biogeosciences
Discussion started: 11 October 2018
© Author(s) 2018. CC BY 4.0 License.

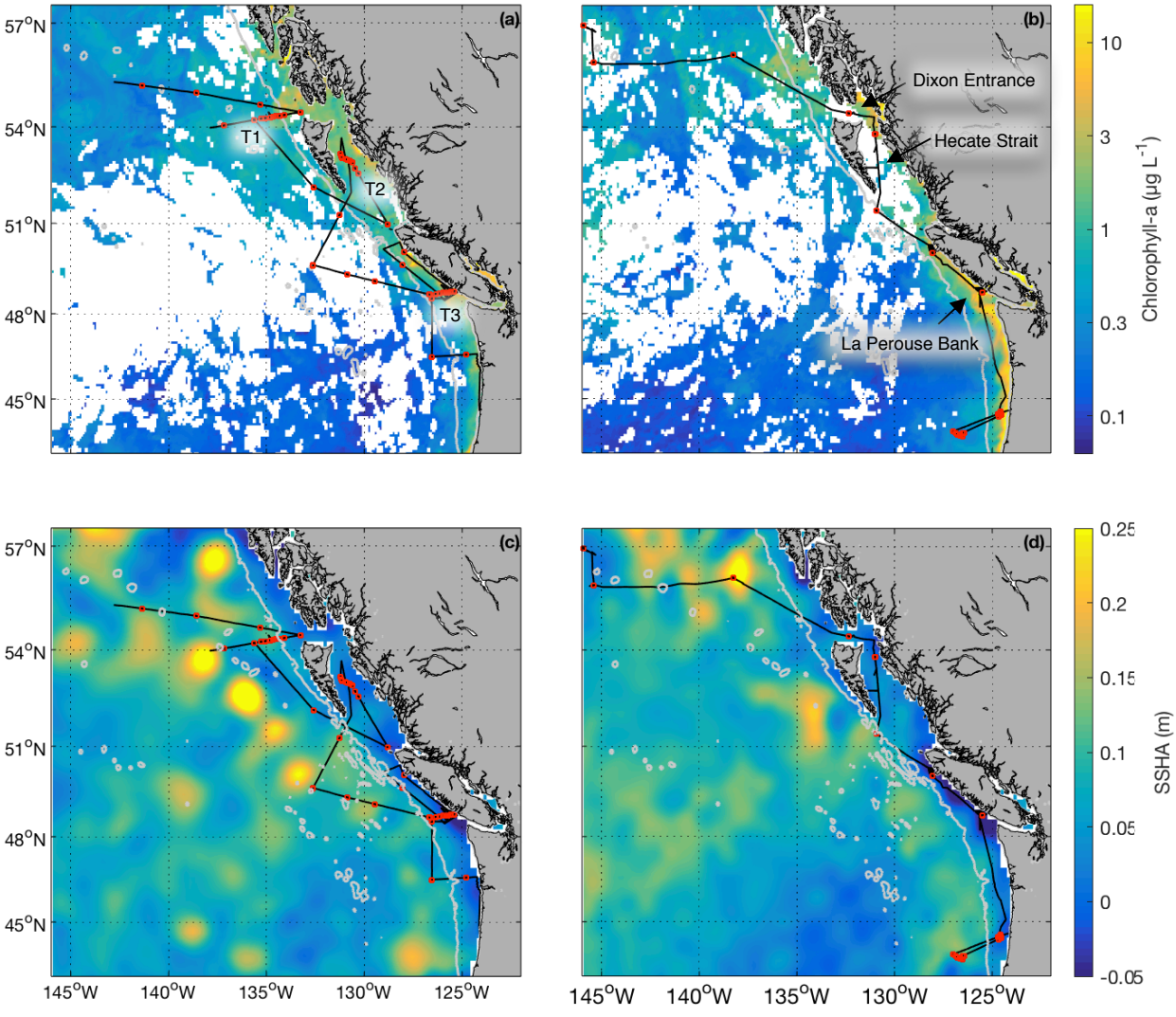

Figure 1. Cruise tracks and discrete sampling stations (red circles) for the July 2016 (O16) cruise (a,c) and August 2017 (O17) cruise (b, d). Panels (a) and (b) show chl-*a* concentration (log scale), derived from AquaMODIS satellite, and averaged over the duration of the respective cruise. Panels (c) and (d) show average sea surface height anomaly (SSHA). Panel (a) shows the location of the T1-T3 transects surveyed during the 2016, whereas panel (b) shows the geographic location of locations of interest. The grey line represents the coastal-oceanic boundary, defined here as the 2000 m isobath.

Biogeosciences Discuss., https://doi.org/10.5194/bg-2018-411
Manuscript under review for journal Biogeosciences
Discussion started: 11 October 2018
© Author(s) 2018. CC BY 4.0 License.

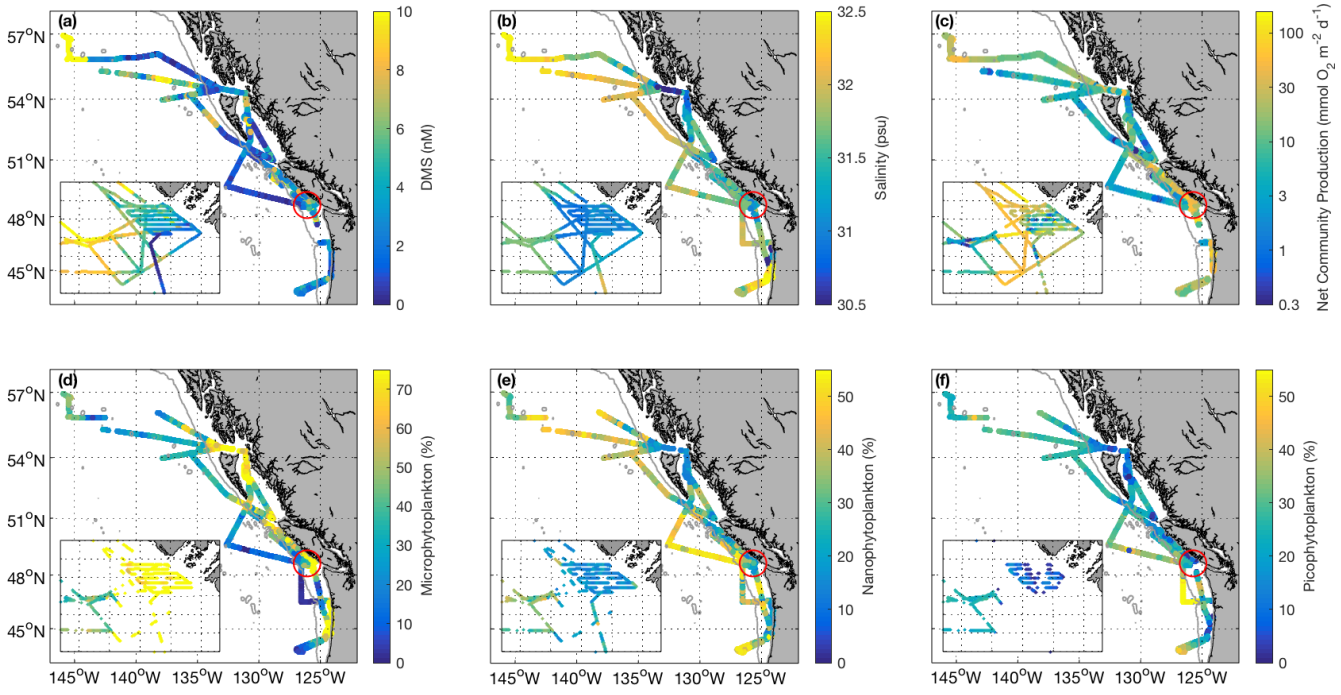

Figure 2. Spatial distribution of DMS (a), salinity (b), net community production (C; note log scale), and micro-, nano-, and picophytoplankton relative abundance (d-f) during the O16 cruise July of 2016 and the O17 cruise August of 2017. Color scaling on the maps are adjusted to ensure readability and best illustrate spatial patterns. Some data values are higher than the maximum scale of the colorbar. The inset box shows the La Perouse Bank region, as marked by the red circle. The grey line represents the coastal-open ocean boundary (2000 m isobath).

Biogeosciences Discuss., https://doi.org/10.5194/bg-2018-411
Manuscript under review for journal Biogeosciences
Discussion started: 11 October 2018
© Author(s) 2018. CC BY 4.0 License.

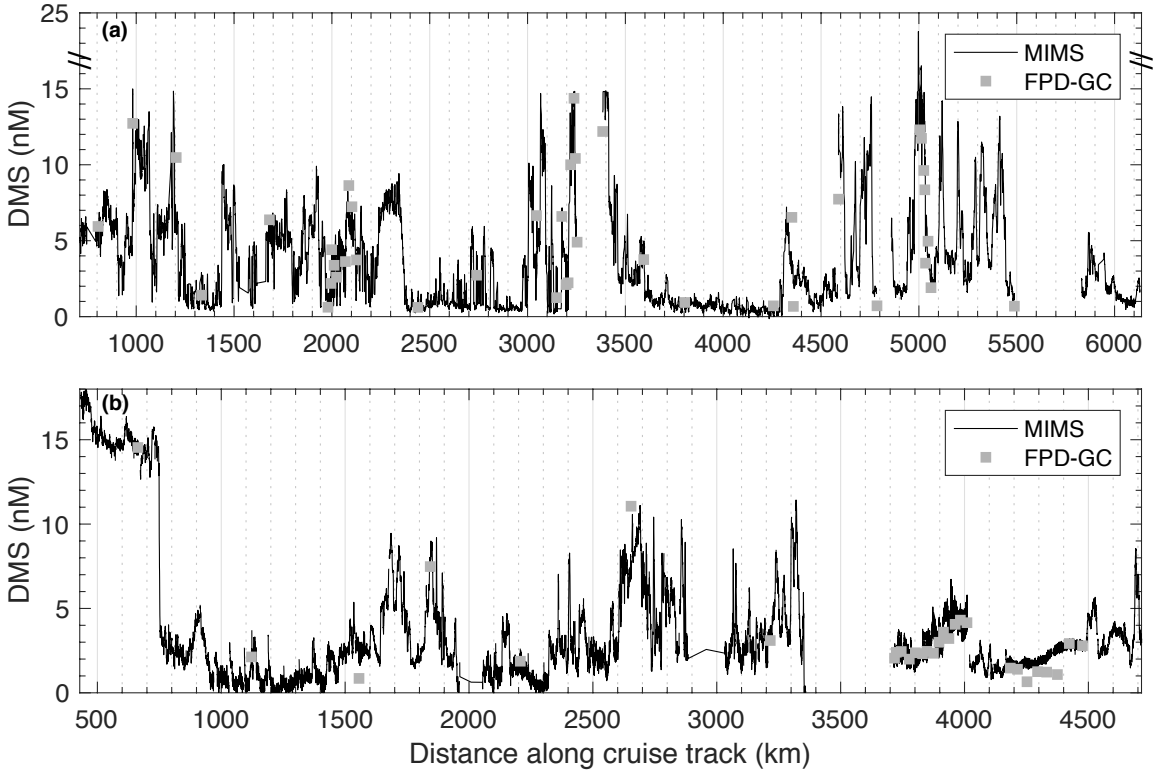

Figure 3. DMS concentrations during the O16 cruise in July of 2016 (a) and the O17 cruise in August of 2017 (b) as measured by membrane inlet mass spectrometry (MIMS, continuous black line) and a purge-and-trap sampling system connected to a gas chromatograph equipped with a flame-photometric detector (grey symbols). Mean absolute error was 0.93 nM for all paired measurements between the two instruments.

Biogeosciences Discuss., https://doi.org/10.5194/bg-2018-411
Manuscript under review for journal Biogeosciences
Discussion started: 11 October 2018
© Author(s) 2018. CC BY 4.0 License.

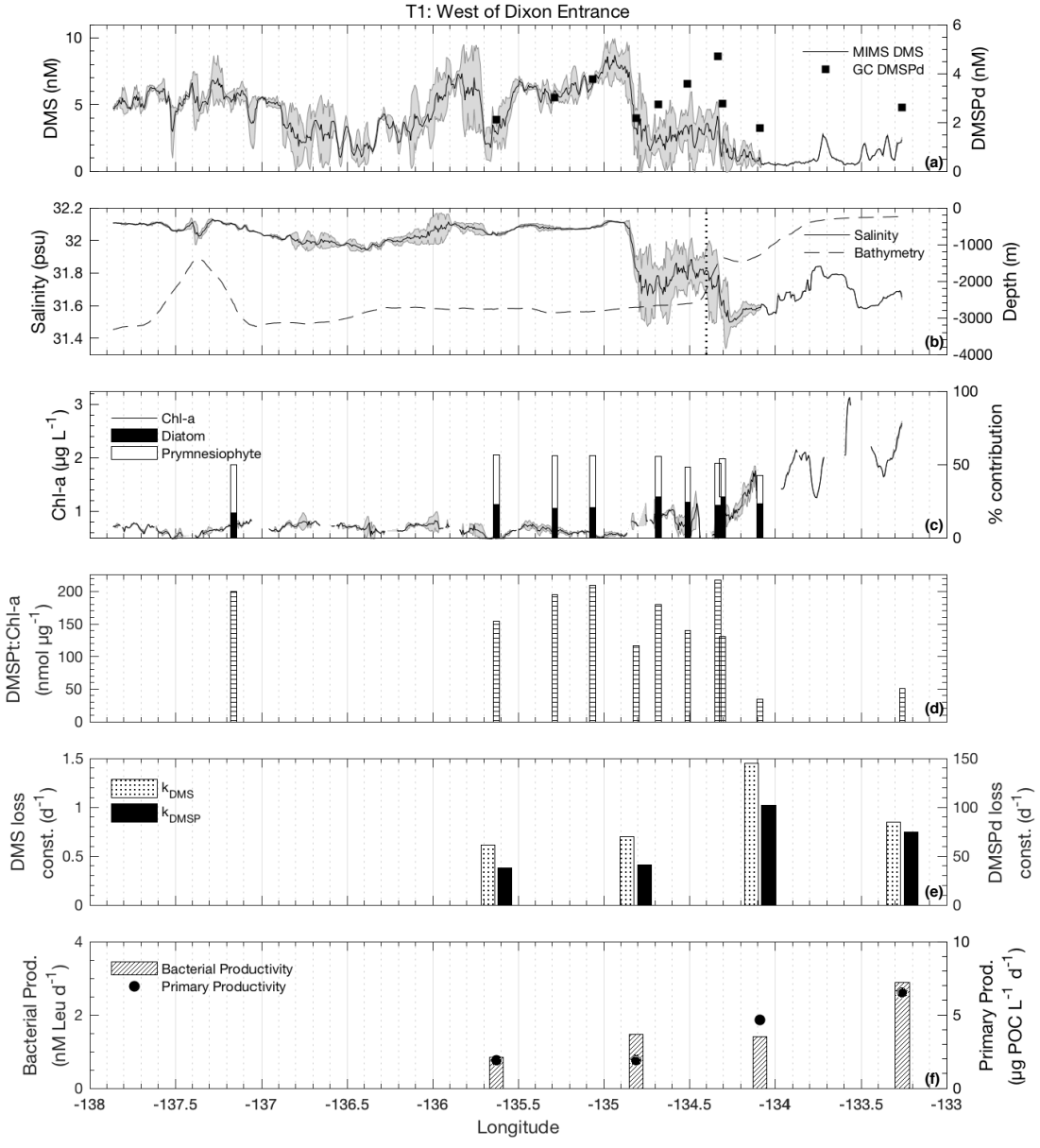

Figure 4. MIMS-based DMS concentration measurements and station-based DMSPd measurements (a), salinity and bathymetry (b), chl-*a* and HPLC-based station estimates of diatom and prymnesiophyte as defined % contribution to total assemblage (c), DMSPt:chl-*a* ratios (d), DMS/P consumption rate constants (e), and bacterial and primary productivity rates (f) along the T1 transect west of Dixon Entrance during July 2016 (O16 cruise). Shaded regions represent standard deviation of repeated measurements across the transect. The vertical dotted line in panel (b) indicates the approximate shelf break (2000 m), at 134.4° W.

Biogeosciences Discuss., https://doi.org/10.5194/bg-2018-411
Manuscript under review for journal Biogeosciences
Discussion started: 11 October 2018
© Author(s) 2018. CC BY 4.0 License.

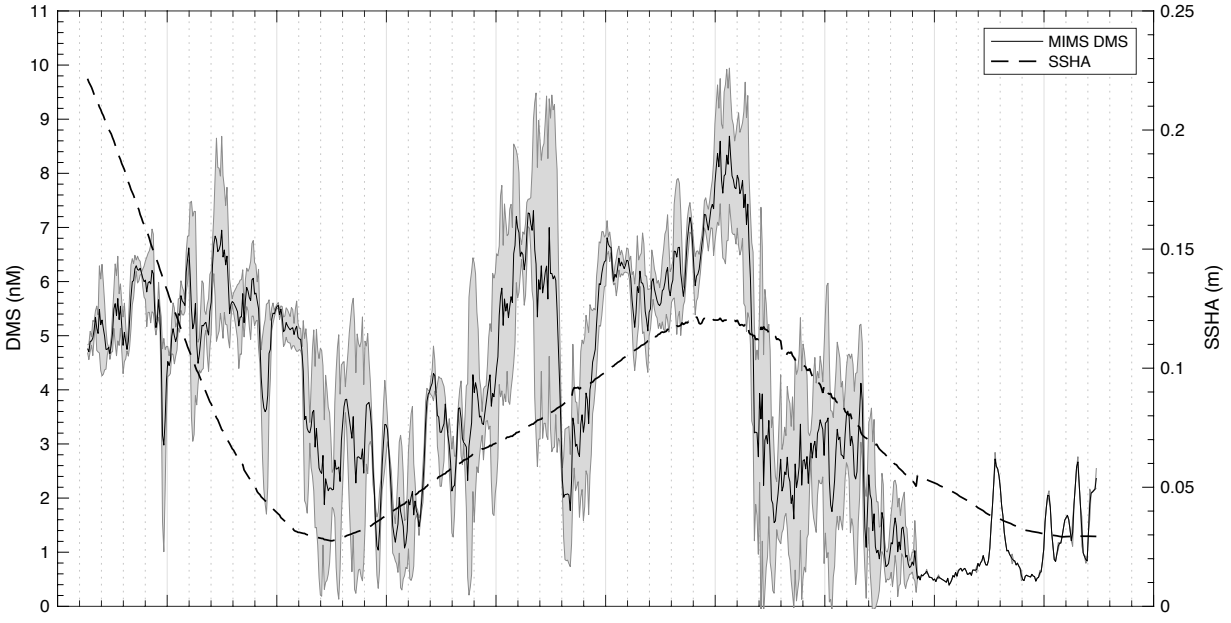

Figure 5. Line plot of sea surface height anomaly (SSHA) on 15 July, 2016 and observed DMS concentrations between 14 July and 16 July, 2016 along T1. DMS along the T1 transect is highest in those areas influenced by positive SSHA values.

Biogeosciences Discuss., https://doi.org/10.5194/bg-2018-411
Manuscript under review for journal Biogeosciences
Discussion started: 11 October 2018
© Author(s) 2018. CC BY 4.0 License.

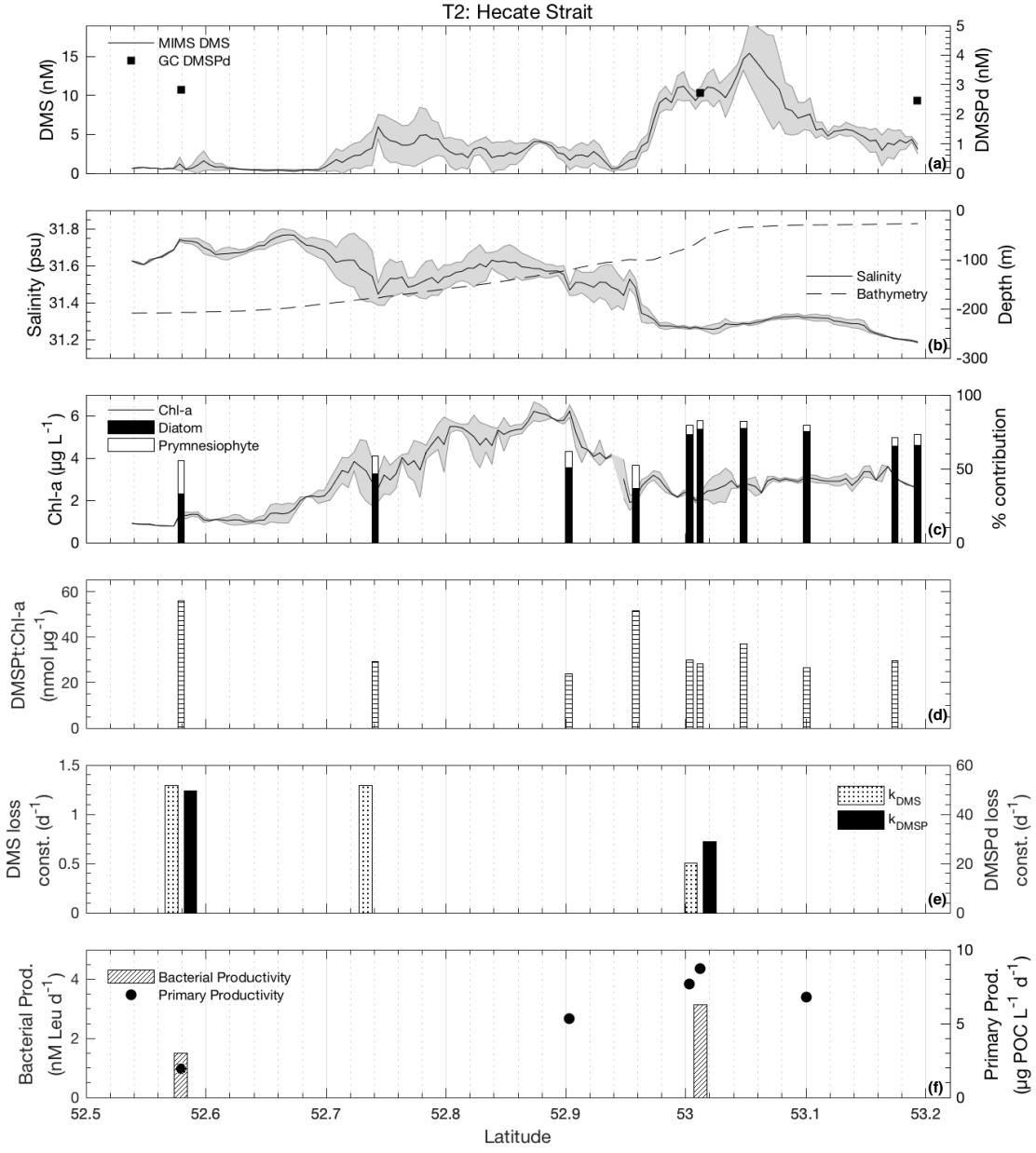

Figure 6. As for Fig. 4, but for the T2 transect.

Biogeosciences Discuss., https://doi.org/10.5194/bg-2018-411
Manuscript under review for journal Biogeosciences
Discussion started: 11 October 2018
© Author(s) 2018. CC BY 4.0 License.

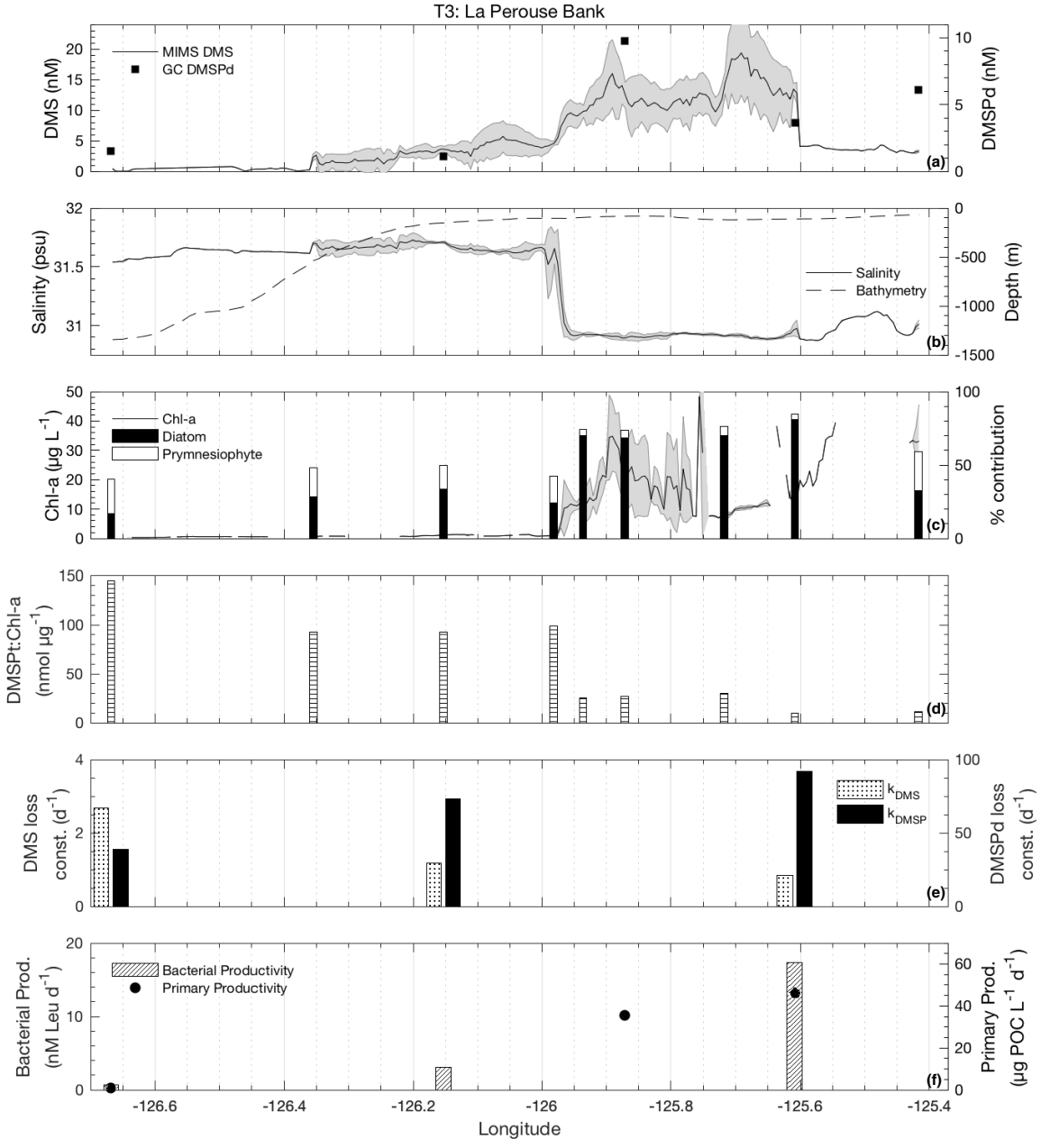

Figure 7. As for Figs. 4 and 6, but for the T3 transect.

Biogeosciences Discuss., https://doi.org/10.5194/bg-2018-411
Manuscript under review for journal Biogeosciences
Discussion started: 11 October 2018
© Author(s) 2018. CC BY 4.0 License.

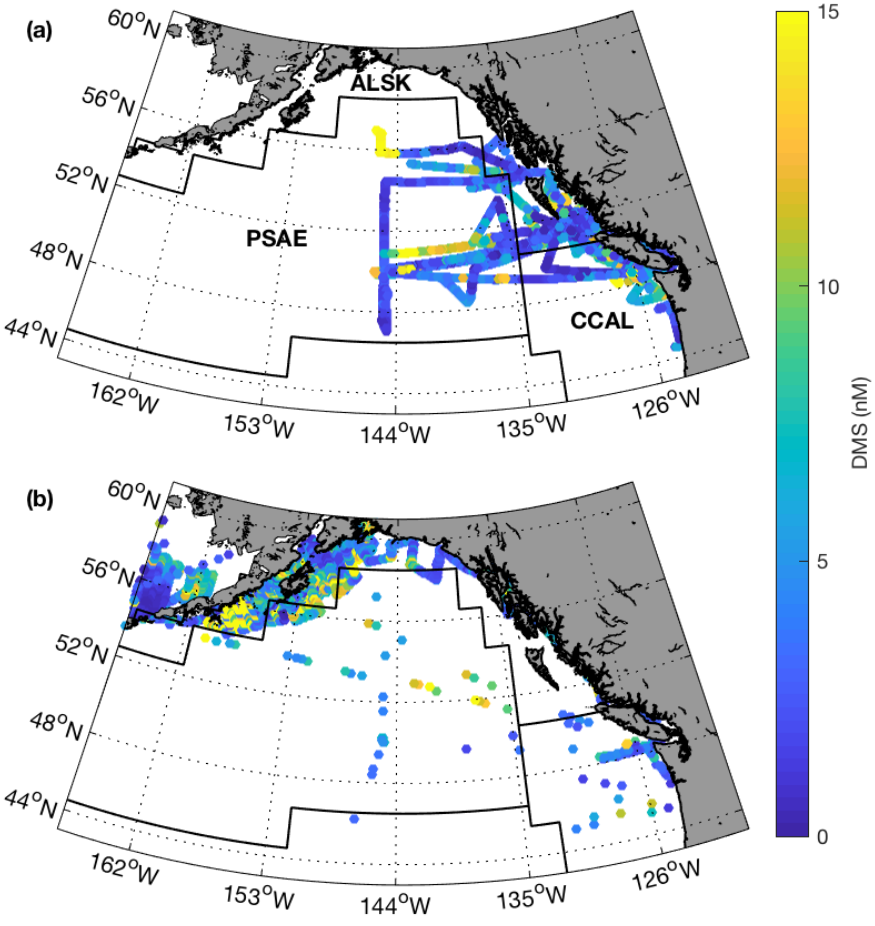

Figure 8. Spatial distribution of summertime DMS measurements from MIMS (a; 2004-2017) and the PMEL (b; 1984 - 2004) data set. Black lines represent boundaries of Longhurst biogeographical provinces, with province names show in panel (a).

Biogeosciences Discuss., https://doi.org/10.5194/bg-2018-411
Manuscript under review for journal Biogeosciences
Discussion started: 11 October 2018
© Author(s) 2018. CC BY 4.0 License.

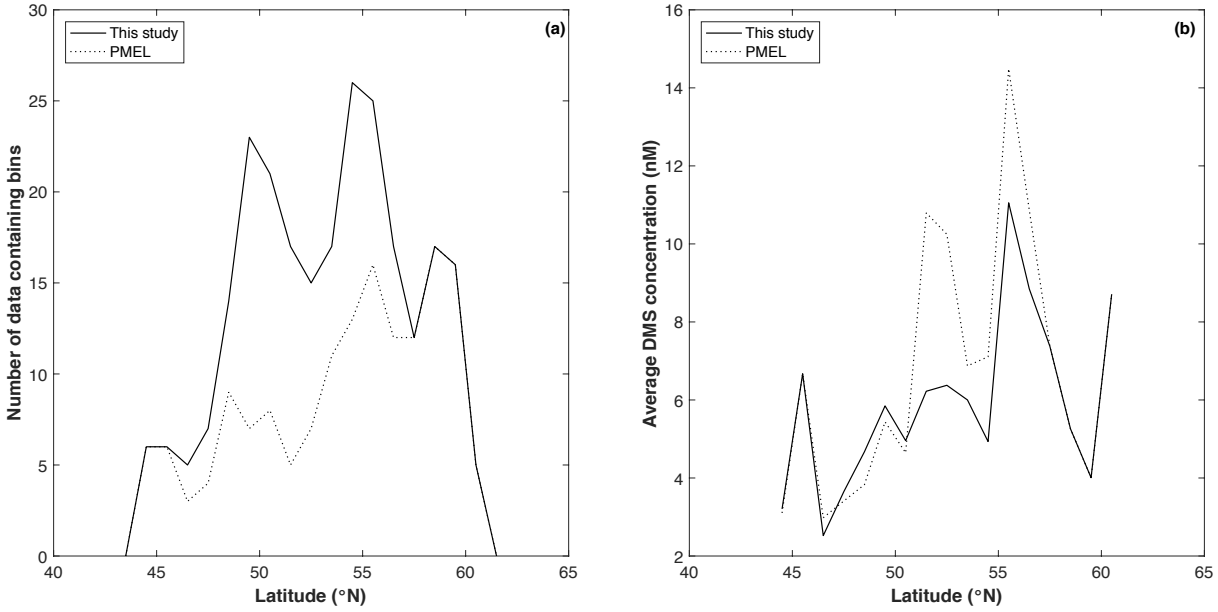

Figure 9. Latitudinal distribution of data containing bins (a) and average DMS concentration (b) for PMEL (dashed line) and combined (PMEL and MIMS) data sets.

Biogeosciences Discuss., https://doi.org/10.5194/bg-2018-411
Manuscript under review for journal Biogeosciences
Discussion started: 11 October 2018
© Author(s) 2018. CC BY 4.0 License.

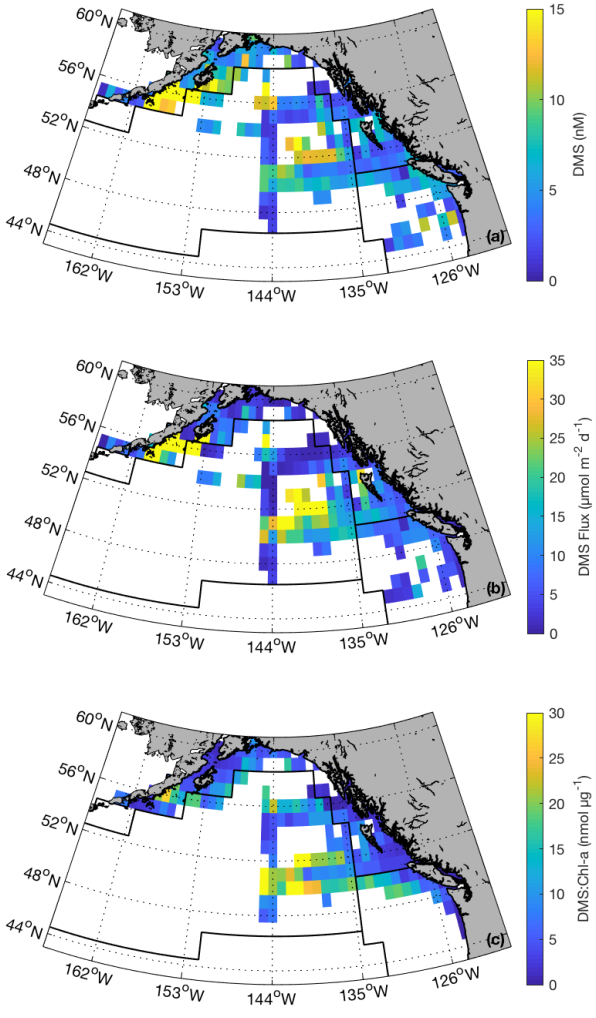

Figure 10. Summertime DMS concentrations (a), DMS sea-air fluxes (b), and DMS:chl-*a* ratios (c) binned to 1° x 1° spatial resolution. These maps were derived using our combined PMEL/MIMS data set (1984–2017; June, July and August). Black lines correspond to boundaries of Longhurst biogeochemical provinces. Maximum values (47 nM, 180 µmol m^{-2} d^{-1}, and 47 nmol $µg^{-1}$ for panels a, b, and c, respectively) exceed the bounds of the colorbars. Maximum values for DMS and DMS flux occur in the waters south of the Alaska Peninsula, whereas maximum DMS:chl-*a* occurs mid PSAE.